THESIS

LIGHTNING CHARACTERISTICS IN BOW ECHO AND SUPERCELL STORMS

Submitted by
Richard Gregg Cullin II
Department of Atmospheric Science

In partial fulfillment of requirements
For the Degree of Master of Science
Colorado State University
Fort Collins, Colorado
Summer 2008

ABSTRACT OF THESIS

LIGHTNING CHARACTERISTICS IN BOW ECHO AND SUPERCELL THUNDERSTORMS

The emphasis of this research seeks to answer a number of questions related to the lightning characteristics and features of both bow echo and tornadic supercell storm types. Initial findings suggest the total lightning characteristics of both the convective uni-cell and squall-line bow echo cases exhibit consistency in that their lightning statistics correlate well against the convective strength of the storm. Repeatedly, the convective strength and lightning maximums precede the bow maximums by an appreciable period of time. Additionally, for squall line bows comprised of multiple cells, this study exhibits that these individual cellular components have lightning characteristics similar to the broader storm and furthermore exhibit intensity maxima preceding the overall storm strength maxima. While an individual cell does not appear to be capable of directly influencing the overall storm lightning activity or related storm strength, a number of cells acting in coordination, and in opposition to the overall storm trend, do possess the ability to change the overall storm lightning profile.

Within the broader view of total lightning, the NBE, or narrow bipolar event, is a newly discovered, unique intra-cloud lightning discharge that has been connected to strong convection. An additional focus examines whether +NBE behavior exhibits a trending similar to intra-cloud and cloud-to-ground lightning, if a relationship exists between +NBE rate and the bowing of the storm, and the physical location of these +NBE events within the bow.

The second portion of the study focuses on extending the knowledge base regarding lightning characteristics, including NBE's, in tornadic supercell cases. This research exhibits that total lightning (IC/CG-/CG+), consistently shows a repeatable depression in lightning rate just prior to and during the time of tornado. The +NBE characteristics of these storms are quite erratic, lending to the inability of the +NBE as a valid storm proxy in these case types.

Finally, a broad spectrum in maximum supercell +NBE rate was obtained. A gross evaluation possibly connecting +NBE rate to geographic location and prevailing synoptic environment was conducted.

Richard G. Cullin

Atmospheric Science Department

Colorado State University

Fort Collins, CO 80523
Summer 2008

ACKNOWLEDGEMENTS

First and foremost I would like to thank the members of my thesis committee. To Drs. Cotton and Chandrasekar, much appreciation for your helpful suggestions and thoughts. I would like to thank my advisor Dr. Steve Rutledge for his leadership and insights throughout the course of this project. He was invaluable in allowing the study to take its unique twists and turns, yet was always mindful in keeping the focus on the overall research goals. I am appreciative of the technical support provided by Dr. Kyle Wiens. At Los Alamos National Laboratory, Drs Jeremiah Harlin and Timothy Hamlin assisted in helping obtain the necessary LASA data for the storm studied. Additionally, I would like to thank Mr. Paul Hein for countless hours of aiding in program coding, debugging, and general IDL help. Certainly, his help substantially reduced the time spent fixing these computer-related problems. Also to the Radar Meteorology Group as a whole; for your general support and advice with a special thanks to Mrs. Brenda Cabell,. Last but certainly not least, to my friends here at CSU for making my experience here a memorable one, and to my family for keeping me calm, patient and always being the constant measure of support and love. This research was funded through the NSF Grant ATM-0649034, and NOAA Grant # NA17RJ1228.

CONTENTS

LIST OF FIGURES

LIST OF TABLES

LIST OF APPENDIX FIGURES

Chapter 1

INTRODUCTION

The two-pronged emphasis of this research seeks to answer a number of questions related to the lightning characteristics and features of both bow echo and tornadic supercell storm types. Since the characterization of the bow echo as delineated by T.T. Fujita in 1978, the past 30 years have seen numerous projects focusing on the dynamical and physical aspects of bow echoes. However, little research has been done in providing an overall view of lightning activity within these storms. A primary goal of this study is to investigate the lightning patterns and trends within bow echoes and to see if there is any connection between lightning activity and the physical bowing of the storm. In analyzing both the convective single-cell bow and the squall-line bow type, we seek to determine if respective total lightning activity is a function of bow type or not. Additionally, for squall line bows comprised of multiple cells, it will be of particular interest to note if these individual cells behave similarly or differently from the overall storm, and their relative contribution to overall storm lightning activity and overall storm convective strength in connection with the bowing of the storm complex.

Within the broader view of total lightning and its various parameters, the NBE, or narrow bipolar event, is a relatively new and unique intra-cloud lightning discharge that has been connected to strong convection, though still largely not well understood. NBE's are very localized, short duration lightning flashes. An additional research focus will

examine whether NBE behavior exhibits a trending similar to intra-cloud and cloud-to-ground lightning, if a relationship exists between NBE rate and the physical bowing of the storm, and the physical location of these NBE events within the bow.

The second portion of the study will focus on extending our knowledge base regarding lightning characteristics, including NBE's, in tornadic supercell cases. Even though lightning in supercell thunderstorms has been fairly well studied, NBE lightning in supercells has not. Therefore, this study looks to reveal characteristics of NBE's in supercells, principally their flash rate and behavior related to storm intensity and time of the tornado. Macgorman and Rust (1998) have spearheaded the research involving characterizations of lightning in tornadic supercells. Their work has shown a number of trends relating lightning behavior to supercell lifecycle. This research seeks to add to the body of that knowledge. Finally, given the results that were obtained from these cases, five bow echoes and five tornadic supercells, an additional question was addressed. Given the geographical location of these storms, ranging from Southern Nebraska to South-Central Texas, it was clear that +NBE rate was not consistent over this large region for storms of similar convective strength. Therefore, a gross evaluation was conducted, to see if NBE frequency was possibly connected to geographic location and the prevailing synoptic environment that exists across this domain. CAPE and 0-6 km shear profiles generated from the Storm Prediction Center (SPC) served to provide the measurements used in this estimation.

Chapter 2 serves to provide a scientific background on both bow echoes and tornadic supercells. Chapter 3 will explain the means by which these storms were analyzed. Chapter 4 will present the lightning and NBE trends associated will all storm

cases and, in addition, show echo volume profiles over this same domain. Chapter 5 will seek to explain the results obtained and offer concluding remarks as to the overall findings of the research.

Chapter 2

SCIENTIFIC BACKGROUND

2.1 Bow Echo Definitions, Classifications and Climatologies

2.1.1 Bow Echo Definition and General Structure

The bow echo was first classified and named as such by T.T. Fujita in 1978. The original figure from his classic paper is shown below (Fujita 1978) (Figure 2.1). Through the examination of radar images looped over the course of a bow echo life cycle, Fujita was able to define five stages in the evolution of this storm type. Additionally he was able to provide a dynamic explanation for the observed resultant reflectivity features. Following from time step A, the convective element started in a linear arrangement, at which time a strong downburst, associated with straight line wind damage, would cause a portion of the storm to be pushed out and away from the rest of the storm elements. This formed the classic bow or crescent shape seen on radar. It was noted that the apex of the bow was strongly connected to the maximum severe winds. Additionally during the physical bowing, the storm usually developed a cyclonic rotation on its northern flank and an anticyclonic rotation on its southern flank. These circulations would later be characterized by others (Weisman 1993) as " bookend" vortices. Following from the peak of the bow, the northern region known as the "comma head" intensified and developed a

hook like shape as the overall storm actually weakened. Fujita observed that the downburst additionally moved to the left side of the storm during this time, and explained

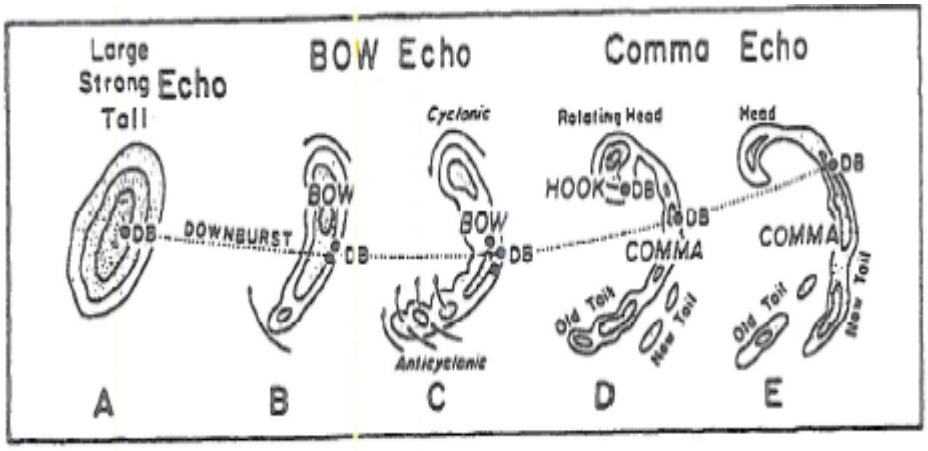

Figure 2.1: Bow Echo Schematic from Fujita (1978).

that this was due to the Coriolis force.

At the time of the study Fujita was unable to identify the origins of this downburst, however a great deal of research has now served to characterize this downburst as the Rear Inflow Jet (Przybylinski and Gery 1983 ; Smull and Houze 1985). This feature is primarily a result of the interplay between the cold pool and the dynamic circulations of the storm, though further research has suggested that these surface winds form as a result of a secondary “updraft/downdraft” circulation induced by the mesocyclone at the bow apex (Bernardet and Cotton 1998).

Though the dynamics of the bow echo have been formulated for quite some time, their appears to be a lack of objectiveness in the ability to classify a bow and its intensity, as determined by the angle the apex creates relative to the two flanks. Fujita did make some estimations of bow intensity given satellite observations (Fujita 1978), however nothing definitive has been produced as yet. Therefore a subjective bow estimation is still the approach currently used, and will be adopted for this current work.

2.1.2 Classification of Bow Echoes by Type

The classic bow echo is in fact a subset of a greater body of convective entities, known as Mesoscale Convective Systems, or MCS's. However, radar observations have shown that bow echoes can be further classified on the basis of their initiation, general appearance, and size. While many different definitions and categorizations have been constructed and described (Przybylnski 1995; Burke and Schultz 2004), the variety of bow echo structures has made identification difficult. To date, the findings of Klimowski et al. (2000) and Klimowski et al. (2004) seem to have provided the most reliable classification schemes. Their research designated 4 group types, the Classic Bow Echo, the Bow Echo Complex, a Cell Bow Echo, and the Squall Line Bow Echo. A representation of these four types can be seen in Figure 2.2.

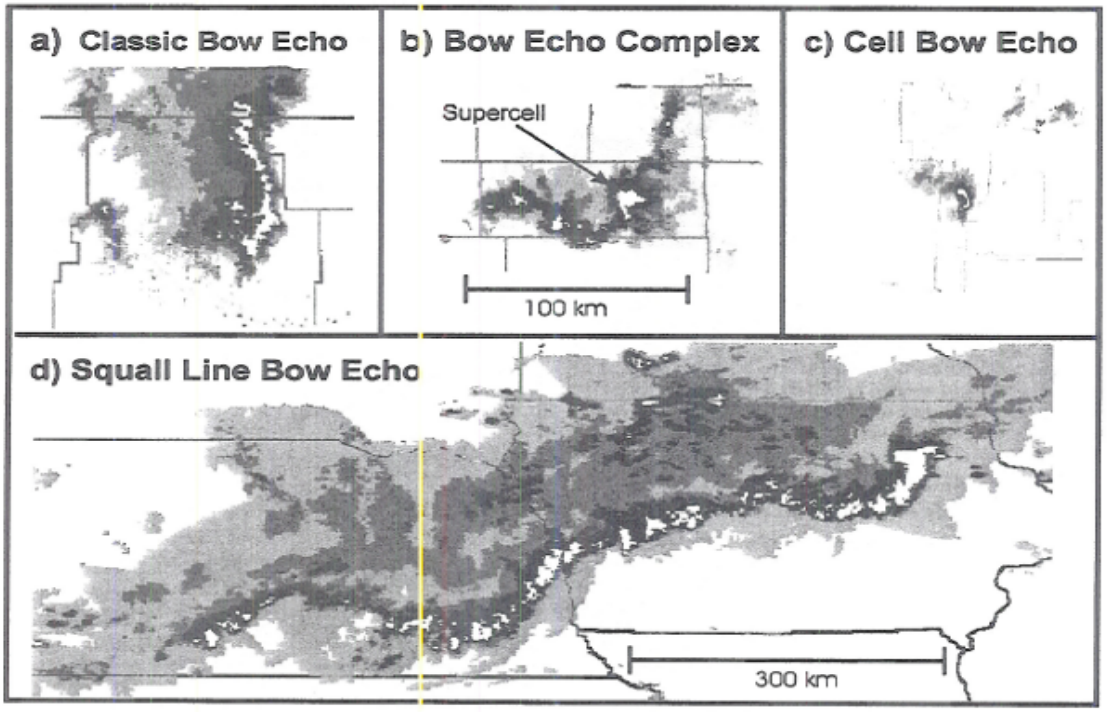

Figure 2.2: Radar reflectivity images of the four bow echo types specified in the text.

The Classic Bow is defined as being seen on a scale larger than an individual thunderstorm, but smaller than a squall line bow, which can extend 100's of kilometers in length. Normally, this arrangement has a trailing stratiform reflectivity pattern and is relatively isolated from other convection. The Bow Echo Complex is similar to the Classic Bow, except that within the convective line, there are several convective types found such as garden variety convection mixed with individual cells arranged in a linear fashion. The Cell Bow Echo is simply an individual storm cell that is bowed; typically these are found on smaller scales than the other 3 types. The squall-line bow is characterized by its sheer length/size as well as the fact that the bow normally occurs within a subsection of the overall convective line. Klimowski et al. (2004) continued to refine their classification by types of initiation and further discussed the dynamical specificities required for each Bow Type.

2.1.3 Climatology of Bow Echo Types:

In order to report the most consistent and current regional climatologies for bow echo thunderstorms, this review will only use the Klimowski et al. (2000) definitions and groupings for bow echoes, given that this is the current research standard. Additionally, the following synopsis focuses only on the Southern and Central Great Plains Regions, as this is the geographical region contained within the LASA lightning detection network used in our study. Although an extensive 4 year bow climatology was conducted by Burke and Schultz (2004), their study used storms which occurred only during the cold season (Oct-Apr). Klimowski et al. (2003) performed a large-scale comprehensive warm season bow echo climatology, but focused primarily on severe convective windstorms over the Northern High Plains; outside the LASA network range.

Klimowski et al. (2004) examined the evolution of 274 bow echoes nationwide, and specifically 40 such events over the Southern/Central Great Plains. Within this subset, 80% were classified as Classic Bow Echoes, 15% as Squall Line Bow Echoes, 5% as Cell Bows and 0% as Bow Echo Complexes (BEC) (Table 2.1). In addition to this region, Klimowski also examined convective windstorms over the Central Plains Mid-Mississippi Valley Region, or (CP-MIS). This region included significant portions of the LASA Network over OK, NE, and KS. Most of these severe wind events occurred in Spring and Early Summer from late afternoon-early morning (Klimowski et al. 2003).

	Initial mode (%)			Final mode (%)					
	WO	SL	SC	BE	BEC	CBE	SLBE	Mergers (%)	Average life span (h)
Northern plains	44	31	25	75	4	7	14	49	3.0
Southern plains	51	33	16	80	—	5	15	53	3.8
Mississippi–Missouri valley	47	47	6	73	1	2	24	55	3.3
Eastern United States	28	72	0	46	—	8	46	54	3.1

Table 2.1: Percentages of Bow Echoes by geographic region evolving from each initial Mode and Final Mode/Bow Type. In initial mode columns WO stands for weakly organized cells, SL for squall-lines and SC for supercells . In final mode columns BE stands for bow echo (classic), BEC for Bow Echo Complex, CBE for cell bow echo, and SLBE for squall-line bow echo.

In terms of convective parameters, it is clear that significantly higher CAPE values exist in the CP-MIS compared to the further north and west Northern High Plains (NHP) region. This was demonstrated by Klimowski et al. (2003) (Figure 2.3). Note that their study includes all convective severe wind events and is not specific to bow echoes, though bow echoes are included. Other studies using modeling techniques have restricted

the environmental conditions for bow echo occurrence with actual numbers, stating that CAPE must be> 2000 J/kg and that 2.5-5 km AGL wind shear must be > 20 m/s (Weisman 1993).

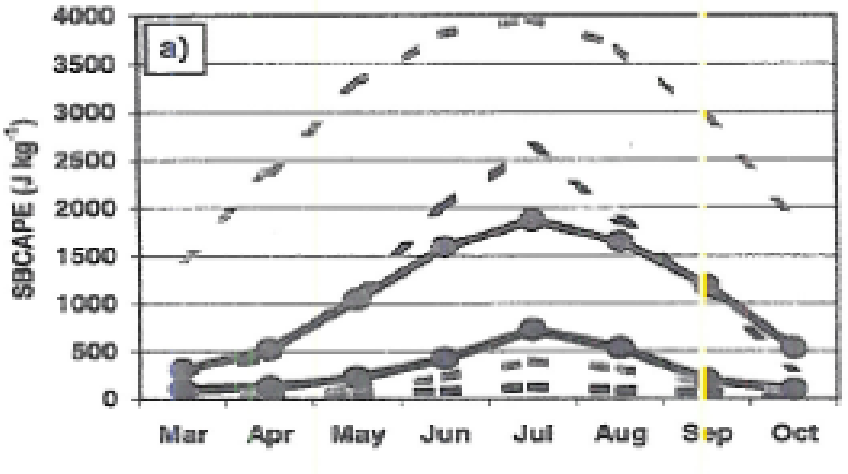

Figure 2.3: Seasonal profiles of a) Surface Based CAPE used in Klimowski et al. 2003. In a), the solid upper line represents CAPE in CP-MIS, while lower solid line is CAPE in NHP. Darker dashed lines represent maximum and minimum CAPE values obtained in each month for NHP, while lighter dashed lines are maximum and minimum CAPE in each month for the CP-MIS region.

2.2 Bow Echo Lifecycle Dynamics and Evolution

2.2.1 Bow Echo Evolution

While most of the research involving storm lifecycle evolution has focused on larger MCS types, such as squall lines, the general circulation features present can apply to the structure of a smaller MCS feature, such as a bow echo. A squall line consists of two basic upper level flow patterns. Specifically, the Front-to-Rear flow starts out as the primary inflow to the storm, is uplifted in the convective line, and then extends back through the stratiform regime (Smull and Houze 1985). Typically, the stratiform regime

forms upwind of the mean flow pattern due to mass advection (Hilgendorf and Johnson 1998). The initial lifting of this flow rapidly cools the air, leading to condensation and precipitation. Weisman and Klemp (1982) (1984) and Weisman (1993) carried out numerous simulations in idealized settings whereby they were able to map the development of a bow echo. At 30 minutes, a maximum updraft generated from this front-to-rear flow was reached, at which time precipitation began to fall and cool the air behind the convective line. This cooler, dense region of air is known as the cold pool (Fujita 1959). The cold pool itself then spreads out at the surface and travels out in all directions. In the case where cold air undercuts warm air inflow, a gust front forms, and additionally can enhance the uplifting of the storm (Weisman and Klemp 1986). The 85 min time point shows that in fact this outflow triggered a maximum updraft of 30 m/s. By 120 min, the maximum updraft had been reduced, however the region of updraft velocity >4 m/s had greatly increased, leading to an increase in precipitation intensity at the surface (Figure 2.4). In a cyclic fashion, this allowed the cold pool to strengthen and feed continued storm growth. Also at this time point, the bookend vortices became apparent on both the north and south flanks of the storm, as did the rear-inflow jet (RIJ). During this intensification the updraft is upright and is much stronger compared to sixty minutes prior. By 240 min, the line has a continuous bow shape extending some 50 km between the bookends. Interestingly, the mean updraft along the convective edge has weakened, yet the RIJ has continued to intensify due to the strengthening of the cold pool and the resultant increase in surface based positive vorticity within the cold pool.

2.2.2 Bow Echo Dynamics

Initially, one must understand the relationship between the vorticity produced by the cold pool and that generated by the ambient shear environment. Their net effect governs the storm appearance and thus its' functional strength. As RKW Theory formulated by Rotunno et al. (1988) is the current standard for explaining this

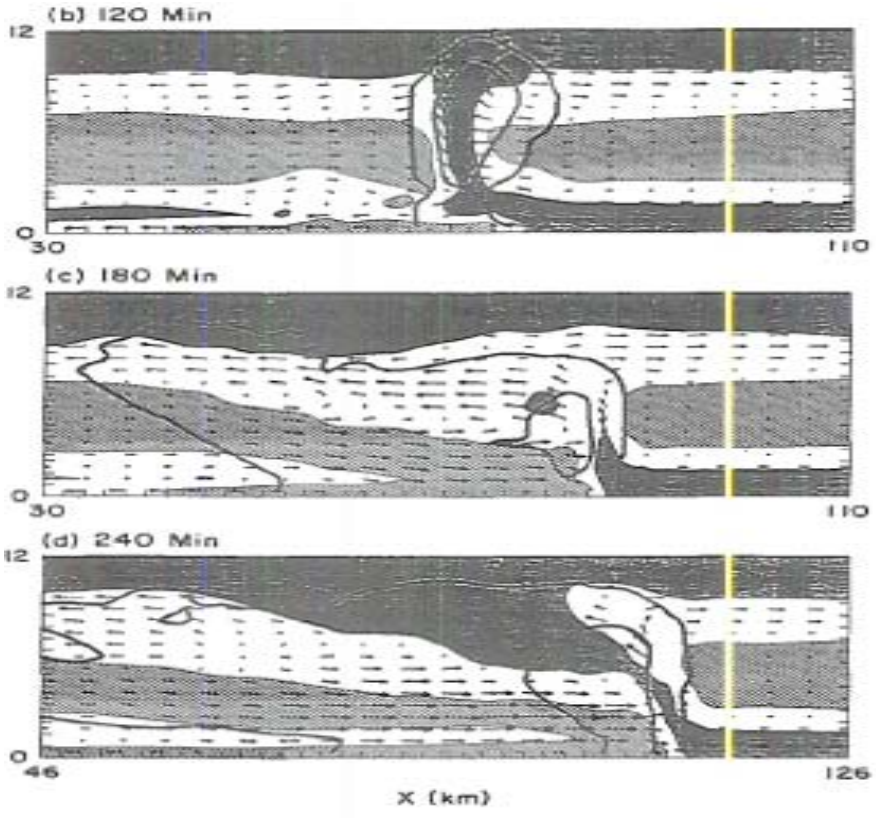

Figure 2.4: A Vertical Cross Section Profile from the Idealized Bow Simulation of Weisman (1993). Of importance, note the light grey area, which is the RIJ and the steady increase in the flow field during these timeframes. Also, note the highest rainwater concentrations, represented by the contours, present aloft at 120 min, but descending to the surface by 180 min. Lastly it is apparent that the primary updraft is weaker in nature at the final timepoint. The 240 min timepoint corresponds to the maximum peak of the bow.

phenomenon, it is truly meant to relate to convective mesoscale convective systems as a whole, and is not specific to bow echoes. Fortunately this theory was applied to bow echoes by Weisman (1992, 1993). Figure 2.5 visually exhibits the explanation put forth. Note that as the cold pool develops, in b) the negative vorticity produced balances the ambient shear and this forces the updraft/storm to become upright. A maximum updraft, followed by the first signs of bowing some 35 minutes later would occur at this point (Weisman 1993). Some time later, the dynamics are such that the cold pool has strengthened and its relative vorticity has overwhelmed the ambient shear, thus tilting the updraft (Figure 2.5c). This resultant circulation now aids in producing a stronger, tighter rear inflow jet (RIJ). With a strong RIJ in place, Weisman concluded that in d) the influx of cooler drier air into the cold pool from the RIJ had strengthened this region to the point where the entire system tilted upshear. This point corresponds to the point of maximum physical bowing. It is noteworthy to additionally discuss Weisman's findings involving bookend vorticity dynamics, as he accounted for the bookends' presence and intensification as a direct result of the vertical orientation of horizontal vorticity produced by the cold pool (Weisman and Davis 1998). Therefore, a strong, vertical updraft alone could cause more intense bookend vortex convection. Note that the Bernardet and Cotton (1998) modeling studies suggested the primary surface winds could also be generated via the presence of an "updraft/downdraft" mesocyclone at the bow apex. Therefore, the findings of Weisman may not be the only dynamical explanation for bow echo straight line wind generation.

2.3 Tornadic Supercells

2.3.1 General Supercell Evolution, Structure

Although tornadoes can form under a variety of conditions, most frequently they occur within a type of convective entity known as the supercell. Browning (1964) was the first to present a conceptual model of this storm type, demonstrating that under strong vertical shear environments warm moist low level air was fed continuously into a single updraft core and driven further by the latent heat of condensation. As precipitation fell to the surface it would induce a cold air descent, classified as the rear flank downdraft. Descending to the surface and then spreading out, this cold air would undercut the warm, moist air out in front of the storm. This general pattern of air movement, Browning concluded, was why these storms were able to independently sustain themselves much longer than traditional thunderstorms. Browning additionally noted along with several other studies (Hitschfeld 1960, Newton and Fankhauser 1964), the preferential development and intensification of supercells that moved to the right of the mean wind as opposed to the left. This conjecture has since been confirmed by a bevy of research, and the dynamics of splitting supercells has been expounded upon by numerous people, using non-Doppler techniques (Fujita and Grandoso 1968), as well as multi-Doppler techniques allowing for 3-D wind field construction and related computer simulations (Ray et al. 1975 Schlesinger 1975).

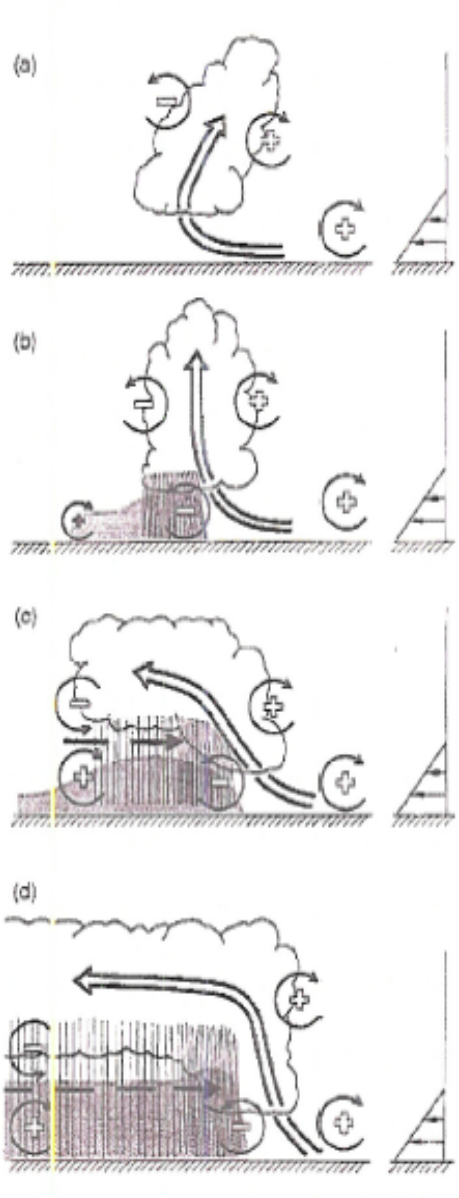

Figure 2.5. A representation of the interaction between the vorticity produced by the cold pool, the ambient shear and the rear inflow jet. The thin circular arrowed lines are representations of positive or negative vorticity. The thick arrow denotes the primary front to rear flow. In a) An initial updraft with no downdraft or cold pool is presented. At time point b) a cold pool has developed and the vorticity generated via this downdraft has forced the storm and updraft vertically. In c) the cold pool has strengthened such that its vorticity is greater than the shear vorticity. The rear inflow jet has increased and the storm tilts slightly upshear. Point d) exhibits the peak strength of the rear inflow jet and a vorticity balance between RIJ and cold pool.

2.3.2 Mesocyclone Formation and Identification

A second distinct feature of all supercellular storms is the confirmed presence of a mesocyclone. This observation was made by surface-based measurements as early as Byers (1942) and Brooks (1949), and later through simulations and radar observations (Lemon 1970, 1976). In a developing supercell, it was first observed that the presence of the mesocyclone was directly attributed to the counter-rotating vortices produced in the main updraft core. As the cyclonic and anticyclonic vortices intensify they produce independent vortex circulations. At this juncture, the storm will split into a left and a right moving storm. Based on the research of Rotunno and Klemp (1982), it was shown that the resulting pressure arrangements favor continued lifting in the right moving piece, as opposed to subsidence from high to low pressure. Given this net result, the right moving storm, cyclonically rotating, will develop a stronger updraft. It should be noted, that a cell-splitting mechanism is not required for the formation of a primary, mesocyclonic updraft. For the isolated cell, simulations performed within Davies-Jones (1984) preferentially demonstrated a cyclonically rotating updraft given a veering of storm-relative winds with height. While tornadogenesis can occur at this time, it is at the third and final stage of supercell development where tornadoes are most likely to occur (Brandes, 1978). This is due to the generation of a precipitation induced rear-flank downdraft, or RFD. Klemp and Wilhelmson (1978) through a series of model simulations were able to recreate this event. They showed that as dry, relatively dense, ambient environmental mid-level air passed beneath the upwind anvil of a storm cloud, it would encounter precipitation falling from aloft and from the periphery of the updraft core (Heymsfield et al. 1978). Evaporative processes would then help initially force, enhance

and maintain the descent of air on the upwind flank (Kamburova and Ludlum, 1966). Surface observations characterize this feature as being associated with strong divergence/spreading located just behind the hook echo (Lemon 1976, Barnes 1978). The outflow from the RFD interacts with lesser downdrafts produced by rain at the surface, combining to form a body of cool air that rushes towards and impinges on the low level inflow. The horizontal vorticity produced could then be advected into the storm updraft, leading to the formation of a low-level mesocyclone. The RFD induces a strong vertical velocity gradient between itself and the updraft. As revealed by Doppler data, the center of this gradient corresponds to the mesocyclone, which has become separated from the updraft core. This mesocyclone movement represents a dynamic shift in its nature, from an updraft only structure to a divided structure, relying on two opposing flow patterns. It is at this mesocyclone center where tornadoes are most likely to touch down (Burgess et al. 1977, Brandes, 1978). Closely related to the mesocyclone, the TVS, or tornado vortex signature, normally appears via Dopplar radial velocity images as a small region (10-20 km) of opposing wind direction (Figure 2.6). Based on radar reflectivity observations, the TVS is concurrent with the classic hook echo pattern and tornado location (Huff et al. 1954). Marwitz (1972) showed the hook echo to be in the strong vertical velocity and temperature gradient somewhat leading the rear-flank-downdraft (Lemon and Doswell 1979).

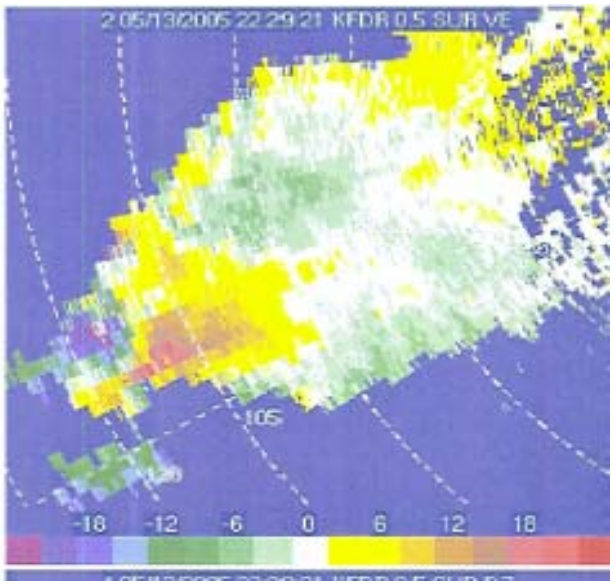

Figure 2.6: Example of a mesocyclone seen via NEXRAD radial velocity image for tornadic supercell on May 13, 2005. Located approx. 115 km from KFDR, Fredrick, OK radar on 0.5 degree PPI scan. Note dark red region corresponding to primary updraft and movement away from radar. This is very close to dark blue/purple region, corresponding to movement towards radar and the rear flank downdraft.

2.3.3 Tornadic Supercell Environmental Parameters

In regards to the thermodynamic parameters present during tornadic supercells, recent work by Rasmussen and Blanchard (1998), Thompson and Edwards (2000) and Markowski et al. (2002), has pointed towards various low level thermodynamic parameters as being particularly associated with tornadogenesis. Rasmussen and Blanchard (1998) found that tornadic supercells tended to have moderate shear and low to moderate CAPE. An increased low level (0-3 km) CAPE in particular lent itself to more favorable tornadic frequency. Thompson and Edwards (2000) reached similar conclusions by using reconstructed Rapid Update Cycle-2 (RUC-2) reanalysis thermodynamic profiles for 321 supercell storms.

2.4 Lightning: Background, Charging Methods and Evolution Within Storms

2.4.1 Lightning Basics: Formation and Charge Type

The body of research has employed both observational and laboratory studies to identify a variety of methods for thunderstorm electrification. Overall, these mechanisms can be categorized as either precipitation-based or convection-based. In the case of precipitation-based charging, charge can either be exchanged by hydrometeors interacting through direct collision or by one hydrometeor splitting into multiple parts (Macgorman and Rust 1998). This mixture of oppositely charged particles would then need to be separated either by gravity/fall speed or convection. In the convective charging hypothesis formulated by Grenet (1947) and Vonnegut (1953), no precipitation is needed for cloud electrification, but rather the space charge (i.e., ions) of fair-weather is used to initiate the process. As seen in Figure 2.7, when convection begins in a), positive space charge from the ambient environment is pulled into the cloud via the updraft. At this point a screening layer of negative charge (2.7b) forms at the edge of the cloud boundary. As the cloud boundary air cools and sinks, it serves to transport this negative charge down towards the cloud base (Vonnegut 1953, 1955). Inflow of positive charge into the cloud continues and a resultant flow develops. In c), the negative charge has accumulated at the cloud base such that the positive charge flux has increased and three distinct layers of charge have developed.

In precipitation-based charging, the charging of hydrometeors can be specified as either inductive or non-inductive. Non-inductive charging is the method primarily responsible for strongly electrifying a storm, and leading to lightning discharge. In this method, the collisions of solid and liquid hydrometeors lead to both charge transfer and

subsequent electric field generation (Kuetnner et al. 1981). Inductive charging occurs when a previously uncharged particle passes through an ambient electric field. The surrounding field "induces" a charge of opposite polarity on the hydrometeor surface, whereby further collisions occur. Therefore, the collision process is involved in both inductive and non-inductive precipitation charging. One can see here how both mechanism types might work together to enhance the overall charge structure.

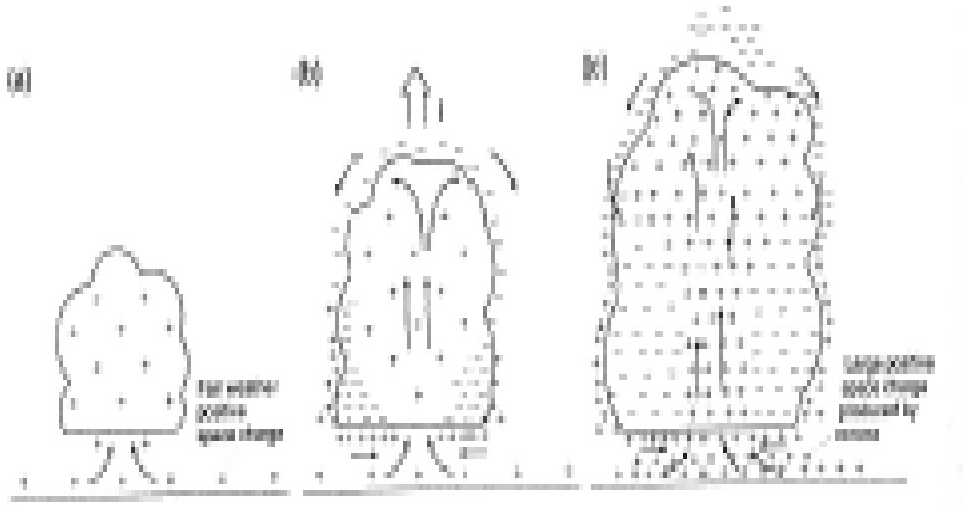

Figure 2.7: Schematic of the convective charging mechanism. In a) the cumulus cloud ingests positive space charge. In b) a negative screening layer forms and an organized transport of negative charge towards the base of the cloud begins. The positive updraft is still occurring. In c) the negative charge at cloud base is large enough to produce corona discharge and subsequent increased flux and density of positive charge into cloud and just below cloud base (From Macgorman and Rust "The Electric Nature of Storms"; originally from Vonnegut 1955)

Specific to non-inductive precipitation based charging, an empirical study by Reynolds et al. (1957) first detected charge transfer in cold cloud layers between graupel pellets and regions containing both supercooled water and ice crystals. Indeed, charge separation in thunderstorms is closely tied to the microphysical interactions of water and

ice particles in the mixed-phase cloud region. Takahashi (1978) showed that sublimating graupel charged negatively and graupel growing by deposition charged positively upon collision with ice crystals. Observations of actual thunderstorm charge structures made by E.R.Williams (1989) and others were consistent with these laboratory findings, giving further support and credence to the microphysical underpinnings. Specifically, negative charging of graupel over a large range of conditions was prevalent, with this main negative region overlaid with a positive charge layer comprised of ice crystals. Williams additionally noted a lower layer of positive charge underneath the main negative core. In totality, the traditional conceptual view of a thunderstorm was developed and visually presented as a classic tripole structure, with positive charge layers above and below the mid-level negative region. Cases involving more than three charge layers and "inverted" charge structures (negative surrounding mid-level positive) have also been identified, (Stoltzenburg et al. 1998, Tessendorf et al. 2006).

2.4.2 Discharge Dynamics and Type

As a convective cell strengthens, the updraft strength of that convection will increase in magnitude. Thus, the supply and transport of condensate being lifted into the mixed phase region of the cloud will also increase. As such, the degree of charging is functionally dependent on updraft strength (Vonnegut 1963). When a storm is ready to discharge, it can do so in two basic ways, either from cloud to ground (CG) lightning or from an intra-cloud (IC) discharge. In the classic vertical tripole configuration, as the primary mid-level negative region grows in amplitude, there are two types of electrical breakdowns. Intra-cloud lightning can be associated with the breakdown between the upper level positive and the mid-level negative charge region. Cloud-to-ground

discharges occur due to the breakdown between the main mid-level charge region and the lower level positive charge zone. Negative polarity CG lightning predominately occurs after this low-level positive charge region has formed (Wiens et al. 2005). Interestingly, another type of –CG lightning, referred to as "bolt-from-the-blue" discharges have been recently noted (Krehbiel et al. 2008). This feature begins as an upward intra-cloud discharge between mid-level negative and upper level positive charge. However, this discharge continues upward, exits the cloud, then directly strikes the ground as a negative leader. Research has shown that the strongest storms favor IC discharges relative to CG lightning. (Boccippio 2002). In terms of positive vs. negative CG discharges, under a classic tripole structure, the negative discharge is expected.

However, numerous field studies have shown that storms can produce predominately positive CG lightning. Dominant positive CG lightning cases have been found in very strong storms associated with an inverted tripole structure arrangement (Williams 2001, Tessendorf et al. 2007 and others). Additional observations have shown that violent storms in general, including tornadic supercells, have a strong tendency to produce predominately +CG (75%-100% of total CG's). (Rust et al. 1985, Stoltzenburg 1998 ,Bluestein 1998, Carey et al. 2003, Wiens et al. 2005). These storms were associated with large hail and rapid increases in radar echo top height. Furthermore, there appears to be a regional trend of higher +CG storms in the Northern High Plains versus other areas of the country (Zajac and Rutledge 2001, Carey et al. 2003).

2.4.3 Lightning Evolution Related to Convective Strength

Building off of Vonnegut's work, there are several field campaigns that have continually linked lightning flash rate to storm updraft strength (Williams et al. 1992,

Rutledge et al. 1992). As reviewed by Macgorman et al. (1989), the literature closely links storm updraft velocity to greater ice production aloft, higher precipitation rates, and higher lightning frequency. Therefore, the lightning parameter has continually been used as proxy to infer storm strength and convective intensity. There have been many different ways in which the research has tried to develop a strict relationship between these two fields. Total Lightning, IC/CG ratio, Total CG, +CG, and even Narrow Bipolar Events have been some of the lightning parameters used to estimate storm strength, each having varying degrees of success (Boccippio 2002, Lang and Rutledge 2002, Suszcynsky and Heavener 2003, Tessendorf et al. 2007, Wiens and Suszcynsky 2007).

Specific to storm type, supercellular lightning profiles formulated by Goodman et al. (1988) agree well with the idea that as the updraft increases, the storm intensity and precipitation increases as does the lightning flash rate. This continues until supercell collapse.

In relation to bow echoes, little research has been done relating lightning characteristics to this MCS type. Rutledge et al. (1990) examined one bow echo MCS and found that positive CG anomalies occurred in the developing stratiform region NW of the convective line. Lang and Rutledge (2006) observed a cell embedded within a larger bow echo as part of the BAMEX field project, and found that the individual cell responsible for generating the highest winds was dominated by +CG lightning. It was determined that this cell in particular possessed an inverted tri-pole structure and that the mid-level positive charge region was lower in altitude (1-2 km), compared to the rest of the MCS convection. They hypothesize that the strong downdrafts associated with the bow echo winds were able to depress this positive charge region relative to the rest of the storm and

create a scenario favoring more + CG and total CG overall. The enhancement of +CG rates relative to straight-line wind damage and physical storm bowing has not been expanded upon.

In terms of tornadic supercells, the most comprehensive review to date has been conducted by Macgorman and Rust in their book, “The Electrical Nature of Storms”. Here they present two distinct but very different lightning profiles for the tornadic supercell. They specify that the profiles differ based on the strength of the tornado. In both the strong and weak tornado cases, (Figure 2.8 and Figure 2.9) the total lightning flash rates increase as the storm gets near the tornadic stage. However, in the strong tornado case, there is a delay in ground flash lightning rate, coupled with a sharp increase in intra-cloud flashes during the time of tornado. Conversely, the weak tornado case experiences sharp increases in both positive and negative CG flash rate over this time-span. They argue that the stronger tornadic case possessed a much stronger and deeper updraft core, and that this hoisting and displacement of negative charge aloft placed negative charge in close proximity to the upper level positive charge region. Therefore, intra-cloud discharge was preferred. The weaker tornadic cases possessed a substantially weaker updraft, an attribute that did not allow for displacement of the main negative charge core. Therefore, the weaker storms experienced a preferential breakdown between the mid-level negative and the low-level positive charge region. Ground lightning flash rates increased as the storm continued to intensify over this timeframe.

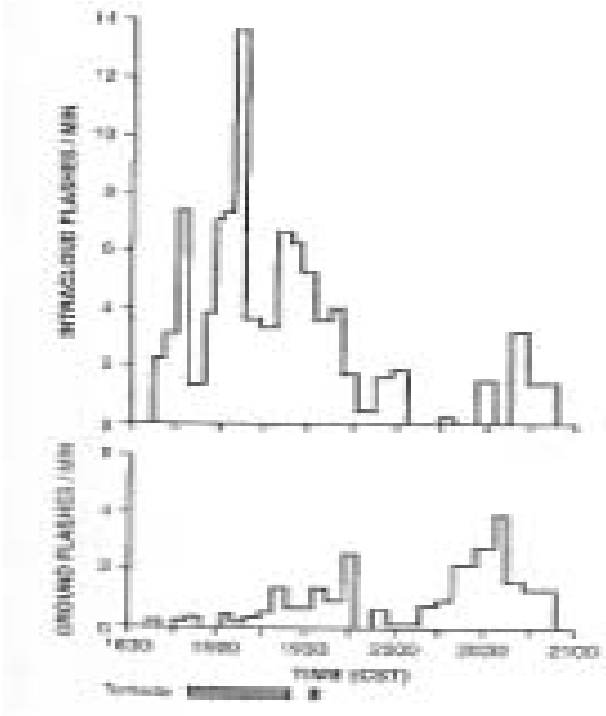

Figure 2.8: Time Series Plots of Intra-Cloud (top) and Ground Flash (bottom) Rates/min for the Strong Binger storm of 22 May 1981. The bars on the bottom indicate when the tornado occurred. (From Macgorman et al. 1989)

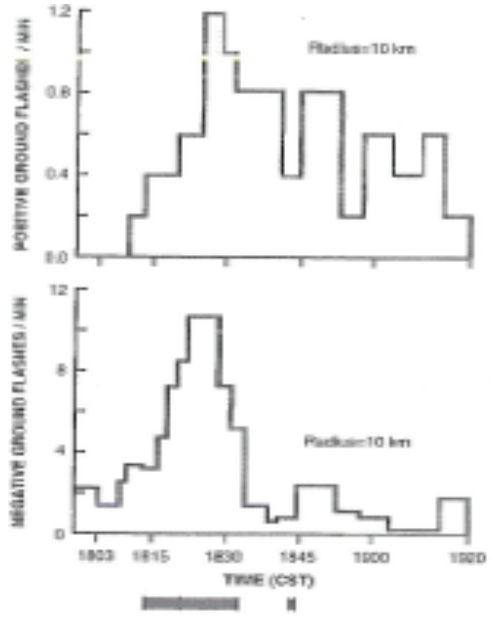

Figure 2.9: Time Series Plots of the Positive (top) and Negative (bottom) Ground Flash Rates for the weaker Edmond OK tornado of 8 May 1986. Bars on the bottom indicate the time of tornado occurrence. (From Macgorman and Nielsen 1991)

2.5 The Narrow Bipolar Event

2.5.1 Background, Identification, Applications

The narrow bipolar event, or the NBE, is a unique, recently discovered sub-type of intra-cloud lightning. They were first detected by Levine (1980) and Willet et al. (1989), and found to emit very powerful VHF radiation pulses. NBE's are distinct from generic intra-cloud and CG lightning based on their specific electric field waveforms. As seen in Figure 2.10, the NBE (2.10b) is distinguished from an ordinary CG pulse (2.10a) by their narrow bipolar pulse widths (approx 10 microseconds), a high signal to noise ratio, and relative temporal isolation from other lightning events (Wiens et al. 2008). NBE classification as either positive or negative is defined as being the same sign of the initial pulse (Wiens et al. 2008). Therefore Figure 2.10 b) is an example of a +NBE. Although temporally isolated, NBE's have been found to occur within the same space as ordinary lightning (Smith et al. 1999). Furthermore, the NBE is not inclusive to the thunderstorm, as several observational studies have shown that not all storms produce NBE's. As an added note, the NBE comprises on average only 0.1% to 1% of all lightning events.

Therefore, the recent focus regarding NBE research has been to more distinctly characterize NBE occurrence and frequency relative to other lightning parameters and radar-inferred storm convective strength. While Suszcynsky and Heavner (2003) and Jacobsen and Heavner (2005) related NBE activity to storm strength, Wiens et al. (2008) offers the first comprehensive study attempting to correlate the NBE to storm strength. While strong correlations were found between total lightning and convective strength, the NBE was not found to be well correlated with either total lightning rate or radar-

convective strength. However, several valuable points came out of this study. Interestingly, about 80% of the recorded NBE's were found to be +NBE's. Also, the data expressed that both + and – NBE's occurred alongside one another. Conversely, previous studies of NBE's in Florida noted an overwhelming dominance of the +NBE overall (Jacobsen and Heavener 2005). Furthermore, a strong connection was noted involving the convective strength of the storms and the 30 dBZ reflectivity contour. As seen in Figure 2.11, NBE occurrence was additionally linked to the 30 dBZ height. This result agreed well with previous findings, suggesting that NBE's typically occur at heights above 10 km AGL (Jacobsen 2003, Rison et al. 1999). As such, the possibility of mapping NBE source heights as a function of convective strength could be justified.

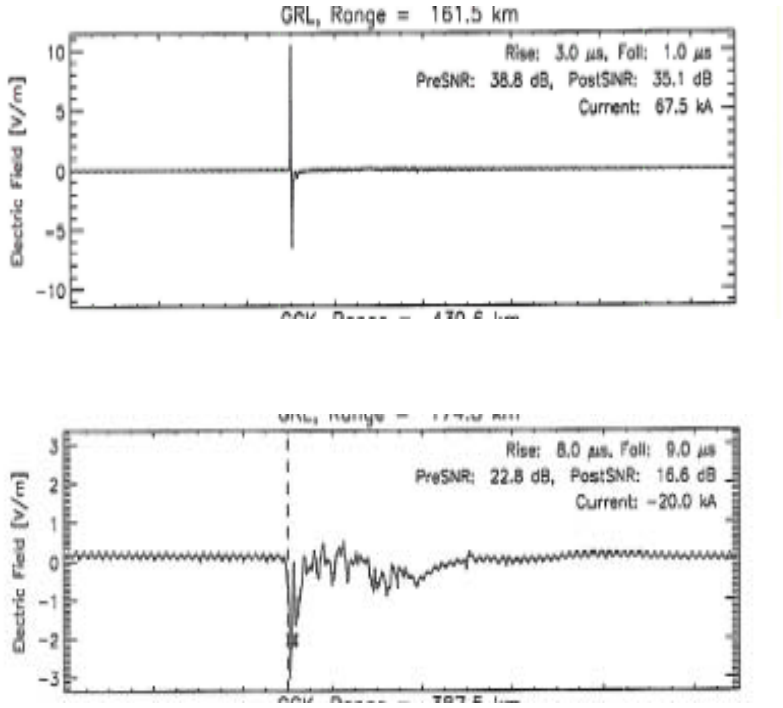

Figure 2.10: Visual of the Waveform Patterns obtained from a Narrow Bipolar Event (a), and a traditional negative Cloud-to-Ground Pulse. (From Shao et al. 2006)

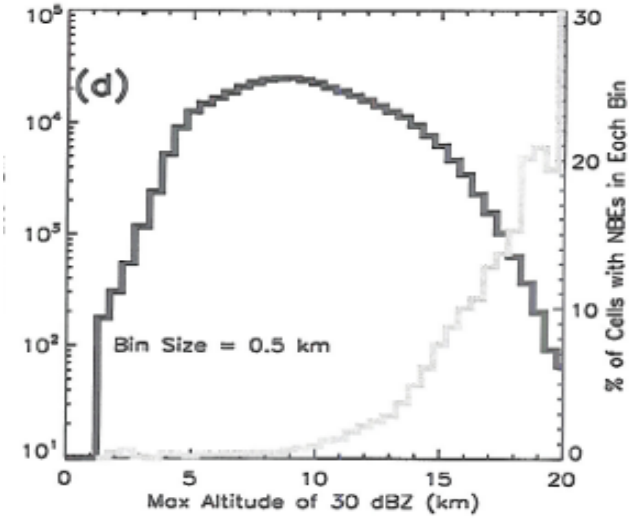

Figure 2.11: Plot of Cell Bin #(dark line) and % Cells w/ NBE (gray line) as a function of the maximum height of the 30 dBZ Reflectivity Contour. Note that NBE's are almost exclusively produced in storm cells with maximum 30 dBZ heights greater than 10 kilometers (From Wiens et al. 2008).

Chapter 3

METHODOLOGY

3.1 Monitoring of Lightning/NBE's

3.1.1 NLDN and LASA Network Background

The two primary networks used to collect lightning data in the following research study were the National Lightning Detection Network (NLDN) and the Los Alamos Sferic Array (LASA). Specifically the NLDN network provides national coverage using a dense network of VLF/HF waveform detectors. The NLDN has shown to be both extremely efficient and accurate for events with peak current >5 kiloamperes; 90% detection efficiency and 500m location accuracy (Cummins et al. 1998). The primary drawback to the NLDN is that prior to April 2006, waveforms were not recorded and only the waveform patterns of CG return strokes were documented. Furthermore, several upgrades to the system in 2003 and 2004 allowed for the waveform criteria to be relaxed. As such, the misclassification of low amplitude IC events as CG events has been detected (Biagi et al. 2006). As of Spring/Summer 2005, the NLDN did not record IC or NBE waveforms. Therefore, the LASA Network will serve as the information source for these events. It bears mention that the NLDN is an operational network, with a primary goal of providing high detection efficiency of CG lightning. The LASA Network is a research-based network, not attempting to provide high efficiency detection for all lightning types.

The LASA Network was installed in 1998 and began with small regional networks in both New Mexico and Florida. The LASA sensors were upgraded in 2004 and in April 2005, the network was expanded to include the West-Central Great Plains. Specifically, these site locations included Lubbock, TX (LBB), Los Alamos, NM (LAM), Norman, OK (OUN), Greeley, CO (GRL), Garden City , KS (GCK), and Lincoln, NE (LNK) (Shao et al. 2006). The map below (Figure 3.1) shows the approximate range and spatial location of the LASA Network. While its detection efficiency relative to NLDN is hardly superb (~ 65 %), it does record IC and NBE events of both polarities, while additionally recording NBE source height (Wiens et al. 2008). Though Wiens et al. compiled NBE activity and profiles for a large number of storms, they included a wide variety of storm types. Thus, no specific study of NBE's in tornadic supercells or bow echoes has taken place.

Given that the storms used in this study ranged from May-June 2005, it was important to have each storm case form within the applicable range of coverage by the LASA network. A slight exception to this rule was made for Bow Echo Case #2, which formed in N. Central Texas and then moved outside of the network range as it evolved. It was determined that this case could be included, provided it did not use the IC lightning profile as a parameter (K.Wiens, personal communication). This points out one key problem with the LASA, the overall low IC detection efficiency. In a recent report, it was estimated that over Central Oklahoma, a location well within the LASA Network, that only 25% of IC's seen by the Oklahoma Lightning Mapping Array were concurrent with LASA (Wiens 2007). This inefficiency is not technological in nature; the system has used fast electric field change sensors since 2002, and improvements have been made to

its triggering, data acquisition and time-tagging systems (Shao et al. 2006). Instead, the main problem is its sensitivity, due to the fact that the network coverage is low in density and that IC flashes are simply lower in amplitude than most flashes. The LASA is therefore biased towards CG detection and varies greatly within the network, based on the event location within the array. Several cases were actually dropped due to a severe lack of IC lightning relative to CG, even though the storm was located within network. Overall, it should be noted that the effective IC/CG ratios for these cases

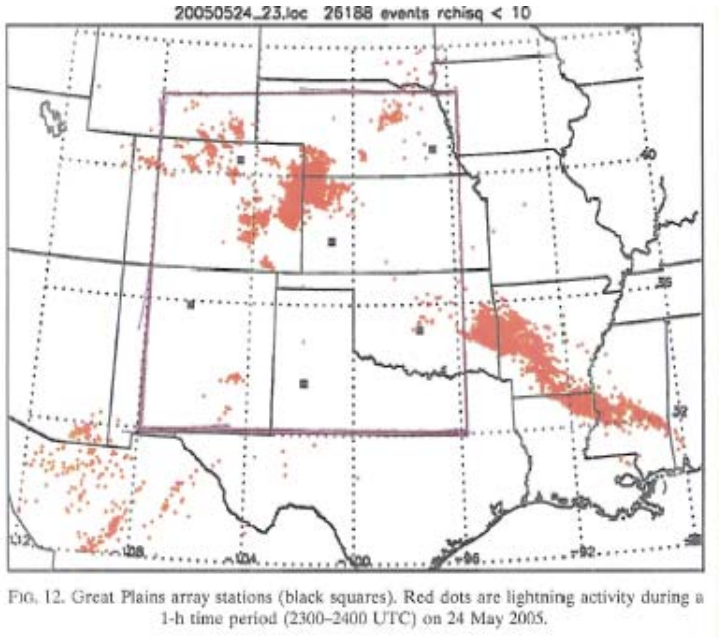

FIG. 12. Great Plains array stations (black squares). Red dots are lightning activity during a 1-h time period (2300–2400 UTC) on 24 May 2005.

Figure 3.1: Great Plains array stations and a general view of LASA Network Range following expansion of network in April 2005. (From Shao et al. 2006)

are likely underestimated. Additionally, detection efficiency can be further degraded if a sensor is malfunctioning and/or non-operational. It was determined that all 6 LASA sensors were fully operational only within the time spans of May 14-16, 19-23, 25-26, 28-31 as well as June 2-4 and 5-30. While it was attempted to use case study selections inclusive only to these dates, there were several cases included on days when the network

was not fully functioning (personal correspondence, K.Wiens). Regardless of operational status, the LASA network is able to identify +/- CG's , +/-IC's, and +/- NBE's based on how the environmental electric field changes when one of these events is generated. The sensors are able to record these waveform patterns and then selectively determine their identity (i.e. the type of lightning). This process is very complex, but this delineation and separation process is quite accurate (Refer to Methology on NBE's for description of waveform identification). For the purposes of this research the IC data was used along with information regarding + NBE frequency. Negative NBE's were not included, as they comprise a very small percentage of the total amount of NBE's. Cloud-to-Ground data was garnered via the NLDN network, which has better detection capabilities for this lightning type. For all lightning types, lat/lon coordinates for each event are provided, and source height information is included in the LASA network output only. This attribute and its application will be further discussed.

3.2 Case Selection/NEXRAD Acquisition

The following is a brief summary, from inception to completion, of the general process that was used to select a case, collect all necessary data, and then effectively apply these results. The first step, case selection, began by going to http://locust.mmm.ucar.edu. These archived radar reflectivity looped images were sifted through and searched for any bow echo or supercell type storms within the year 2005. Specifically, the desire was to find storms on the dates LASA was fully operational, but in an overall sense find storms in the months of May and June. For bow echoes, there was a need to include two types of bow echoes, both the individual cell type and a squall-line type consisting of multiple cellular components. Two individual cell types and three such

squall line cases were found which fit the criteria of location within the LASA Network as designated in Figure 3.1. Forming within the Southern and/or Central Great Plains (TX,OK,KS,NE, NM, Eastern CO), a sufficient total storm time of at least two hours, and a noticeable bowing and linearization cycle were also required. For supercells, the process was slightly more involved in that it needed to be determined if said cell was in fact a supercell, through radar-based mesocyclone detection, and whether or not it was tornadic in nature. For each convective cell, the Storm Prediction Center's database for wind/hail/tornadoes was consulted for the date, time, and lat/lon in question. If a tornado was visually confirmed and reported for the convective cell in question, then the case was retained for analysis. It should be noted that some of the cells thrown out may have produced a tornado, but was not confirmed via a visual sighting. Additionally, before its supercell status could be confirmed, the cell needed to be plainly separate from other convection for at least one hour before and after the time of tornado, or TOT. Given these conditions, both the selected bow echo and tornadic cases were found in a NEXRAD radar database. For the given date/time of each case, the closest NEXRAD radar to the storm in question was selected and the radar information downloaded from http://hurricane.ncdc.noaa.gov. This included radar reflectivity, radial velocity and spectral width fields at time intervals approx every 5 minutes. In a few instances, multiple NEXRAD radars needed to be acquired for a single storm such that the event could be effectively visualized and tracked. For all cases, Table 3.1 below lists the date/times and stations used. The general procedure for viewing these images was to first make a directory for each case and then uncompress/unzip these individual files. Following this, the data was translated into Universal format. These Universal files were successfully

made for all cases and were made at 15-minute intervals over the duration of the storm. These files were turned into subsequent .sweep files. It was only after this manipulation that the program SoloII could be called upon to properly read and visually present the radar data. It was only at this juncture that possible supercell cases could be analyzed for the presence of a mesocyclone, using the radar radial velocity image profiles (See section 2.3). Luckily, all the tornadic cases initially selected possessed a mesocyclone and therefore this procedural loop did not have to be continually repeated.

Storm Type	Type/Tornado Strength	Date	Time (UTC)	Station/s
Bow Echo #1	Convective Cell	June 7. 2005	0:00Z-1:15Z and 3:15Z-8:00Z	KFDR (Fredrick OK)
Bow Echo #2	Squall-Line	June 1, 2005	5:30Z-11:00Z	KDYX (Dyess,TX) and KEWX (San Antonio, TX)
Bow Echo #3	Convective Cell	May 7, 2005	6:45Z-9:15Z	KDDC (Dodge City, KS)
Bow Echo #4	Squall-Line	May 13, 2005	3:15Z- 5:45Z	KFDR (Fredrick, OK)
Bow Echo #5	Squall-Line	May 24, 2005	8:00Z-12:00 Z	KICT (Wichita, KS)
Supercell #1	F0	June 2-3, 2005	22:30Z-2:00Z	KGLD (Goodland, KS)
Supercell #2	F1	May 11, 2005	21:15Z-24:00Z	KGLD (Goodland, KS)
Supercell #3	F1	May 13, 2005	21:30Z-23:30Z	KFDR (Fredrick, OK)
Supercell #4	F3	June 2, 2005	21:45Z-23:45Z	KFTG (Denver, CO) and KGLD
Supercell #5	F1	June 9-10, 2005	23:15Z-1:15Z	KDDC (Dodge City, KS)

Table 3.1: Listing of Bow Echo and Tornadic Supercell Cases Used for Study.

Given these reflectivity images, a number of additional tasks could now be performed.

3.2.1 NEXRAD Applications and Connection to Lightning Data

For each 15-minute interval across every storm, a number of criteria needed to be met by each radar image. Essentially, an overall quality control of the radar data was conducted. First and foremost, the lowest scan angle (0.5^{o}), as well as each increasing angular sweep up to 19.5 degrees needed to show a complete radar image of the storm in question. Some cases needed to be dropped because there were large gaps in the reflectivity patterns at a variety of heights. This may have been a result of error in either the initial radar processing or perhaps post-processing. This would have induced large statistical errors when reflectivity echo volumes were later calculated. In fact, the first three hours of Bow Echo Case #2 needed to be deleted because of this issue. Next, there needed to be strong evidence suggesting that the entire storm was being captured from top to bottom. Therefore, for each case, at its maximum range away from the particular NEXRAD, it was calculated how high in the cloud the radar beam was looking based on the lowest angle sweep of 0.5 degrees. If the height was greater than 1.5 km at any point, it was then surmised that the radar was likely missing a significant portion of the storm, and these cases were discarded. This was a sizeable problem, as many cases began too far away from a particular radar to be reliable. Also, it was preferred that the entire bow/cell be captured by one NEXRAD radar. Following this overview, the cases were individually tracked at the lowest elevation angle sweep and latitude/longitude boxes were assigned for each radar volume time over the storm duration. Specifically for the bow echoes, the lat/lon boxes were constructed in order to capture the primary convective line but not

include the stratiform region/comma head portion of the storm. This consistency was kept so as to prevent anomalous lightning data in this region, such as high +CG rates from the stratiform region, which would influence the overall lightning profiles (Rutledge et al. 1990). For the squall-line bow echo cases specifically, individual cells were "boxed" and followed along with the entire convective line. In the case of the tornadic supercells, the latitude/longitude boxes were made so as to create a 30 x30 km box around the centerpoint of the mesocyclone. This procedure was loosely based off the work of Macgorman and Rust (1998) who employed a 15 km x15 km box around the "meso" to focus its lightning data acquisition. Due to the fact that the range ring intervals were every 15 km, it was difficult to consistently view the matching radial velocity radar image, identify the mesocyclone, and then overlay this region overtop the NEXRAD reflectivity. In a few cases, the radial velocity images could not confirm a mesocyclone. This problem however, only occurred either at the very beginning or very end of each storm, and was well removed from the time of tornado. In these instances, other radar features, such as the hook echo were used as a rough estimate for mesocyclone location. Additional refinements to this procedure included making sure that the km to lat/lon conversion changed for each storm case, given its location. While one degree of latitude change= 110.72 km everywhere, 1 degree longitude can be equal to a wide range of km distances, due to the earth's curvature, and is strongly dependent on N/S location. Therefore, this conversion was case-dependent, and ranged from 87.5 km to 104 km. With all of the lat/lon coordinates recorded, the NLDN and LASA networks could be searched and the lightning data whittled down to individual lat/lon boxes for every 15 minute interval. In the case of the LASA data, it was delivered courtesy of Los Alamos

National Laboratory; specifically J.Harlin and T.Hamlin at 5 minute intervals. For this LASA material, the same lat/lon was used for each five-minute segment within the larger 15 minute timepiece. The final application of the raw NEXRAD reflectivity images was to create, for the bow echoes only, a subjective bow index, whereby each image was assigned a number between 0-10 estimating its bowing angle. Certainly this technique possesses the ability to introduce error into relating bow echo curvature to lightning activity. However, given the lack of an objective technique, this was the best approach.

3.3 NLDN/LASA Lightning Applications

The NLDN was used only to determine Cloud to Ground lightning statistics given its high detection rate (~90%). The research body has suggested that any strike over 10 kA is likely a CG strike. This lower threshold value prevented high amplitude IC events from being mislabeled as weak CG events (Biagi et al. 2006). The overall procedure was such that the appropriate date/time for each storm in the NLDN database was referenced. All 2005 NLDN data were already located on the group server, so a direct copy of daily datasets was made. The search was further refined based on lat/lon, and each 15-minute data segment was copied to a separate spreadsheet. The final distinction was to erase all strikes < +/- 10 kA. A strike number was recorded and a resultant profiling over time of +/- and total CG could be formulated for each case. In the case of the LASA data, the lightning data acquisition itself was not any more difficult, however it took much longer to develop an accurate profile of total IC and positive NBE's. Procedurally, finding date/time and corresponding lat/lon's were not difficult. Separating these data streams into individual 5 minute segments for each lightning type, garnering the necessary lightning information, and then recombining into 15 min intervals was tedious and time

consuming but altogether straightforward. The real problem came when it was realized how the raw LASA was grouped/configured. Essentially, in its base form the LASA data records every “event” occurring, which is very different from every “flash”. It was noted after fully processing several cases that all of the lightning parameters were exceptionally high, with some frequencies on the order of 150-200 events/minute for intra-cloud flashes and CG rates approaching 75/min. This unphysical result was being obtained because in fact one flash was being seen as multiple electric field changes related to the physical processes which occur prior to the actual strike (leader formation/discharge/charge ionization etc.). To correct this problem, an algorithm provided by K.Wiens was applied so as to group these multiple events, (events separated in time by less than 0.5 microseconds and 10 kilometers in space) into one distinct event/flash. With this change made, the lightning flash rates were much more reasonable. At this juncture, the total IC rates and +NBE rates were recorded and a profile for each case was constructed. Although not included in the finalized research, the LASA data was also applied to assess the possibility of using NBE source heights as a plausible means to follow the convective evolution of a given storm.

3.4 NBE Source Height Findings

In its most basic explanation, any electric event carries with it an electric field pulse, and this event is recorded. However, this electric field pulse not only travels in a straight line to the sensor, but also up and down. Therefore, there are two delayed pulses that reach the field sensor at a point just after the primary pulse. These minor pulses correspond to electro-magnetic waves reflecting off the ground, and also reflecting off the ionosphere before traveling to the sensor. Because the time delay between main pulse

and subsequent pulses is related to distance from the sensor, the LASA computers are able to calculate a straight line range and height. This seems straightforward, however, in analyzing the waveform patterns used to conduct these calculations it is plainly obvious that a number of errors and inaccuracies induced several erroneous source heights. In several instances, source heights < 3 km or greater than 20 km were noted. As troposphere heights do not reach this level, these 20+ values were immediately discarded. For the remaining waveform patterns, one needed to literally go through each individual NBE event and determine if the waveform was “clean”, the two minor pulses were visible after the primary pulse, or “dirty”/indistinguishable. As seen in Figure 3.2, this process was extremely subjective. In the following images, some stations appear to have “clean” responses, while specifically the GRL site has a lot of baseline noise, which makes the pulses impossible to individualize. Upon personal correspondence with K.C. Wiens (2008), it turns out that this stations baseline was contaminated by noise from a nearby WWV signal source. A filtering algorithm has since been applied to correct for this constant frequency source. Therefore, this case calculated a believable source height of 8.3 km, and the event itself could be considered clean, given the application of this filtering algorithm. Nevertheless, one bad trigger site could cause a case to be dropped due to intermittent noise. Certainly, this subjectivity may have caused the overall data set to be slightly skewed. Overall, when the final height averages were calculated it turned out that the Standard Deviation of these individual averaged peaks were too large to develop or obtain a reliable profile for any of the cases.

3.5 NBE+/CG+ Misidentifications

In the STEPS 2000 field campaign, it was discovered that an appreciable number of NBE+ events were misidentified by the NLDN and labeled as positive CG strikes (Tessendorf et al. 2007). A secondary analysis conducted with these lightning events sought to confirm if these misidentifications should be considered an ongoing, continuing issue. Based on the findings obtained, less than 1% of all +NBE ‘s were found to be coincident with an NLDN positive CG strike, in the cases analyzed. It should be stressed that this result is extremely case-dependent, as storms producing large numbers of NBE’s and little to no +CG, could be at greater risk for such misidentifications.

3.6 Echo Volume Profiling: Summary

Following completion of the lightning profiling and associated analyses, the echo volume profiles for each storm case were constructed. The procedure for these calculations employed using a variety of IDL programs borrowed from Ms. Brenda Cabell to take a three dimensional snapshot of each reflectivity image for every elevation angle for every 15 min timepoint. The program was able to then integrate and add up the total volume of reflectivity seen greater than 30,40, and 50 dBZ within the storm. This result set was key towards providing a quantitative measure of convective intensity, and comparing these mappings against the lightning profiles already made. It should be noted that all universal radar files needed to be converted into a .cdf format, prior to this application. These echo volume profiles were developed for each bow echo case overall and the selected individual cells within the squall bow cases. Echo Volume (EV) Profiles were also made for each tornadic supercell case, attempting to consistently apply these calculations on the same 30x30 km box used for prior lightning analyses. Figure 3.3

shows an example output, showing profiles at the 30, 40, and 50 dBZ levels. Note that 30 dBZ values were not used in further analyses based on the fact that this reflectivity may be a direct representation of stratiform rain inclusion. Thus, the 40 and 50 dBZ echo volume profiles provide the most consistent quantitative measure of convective strength.

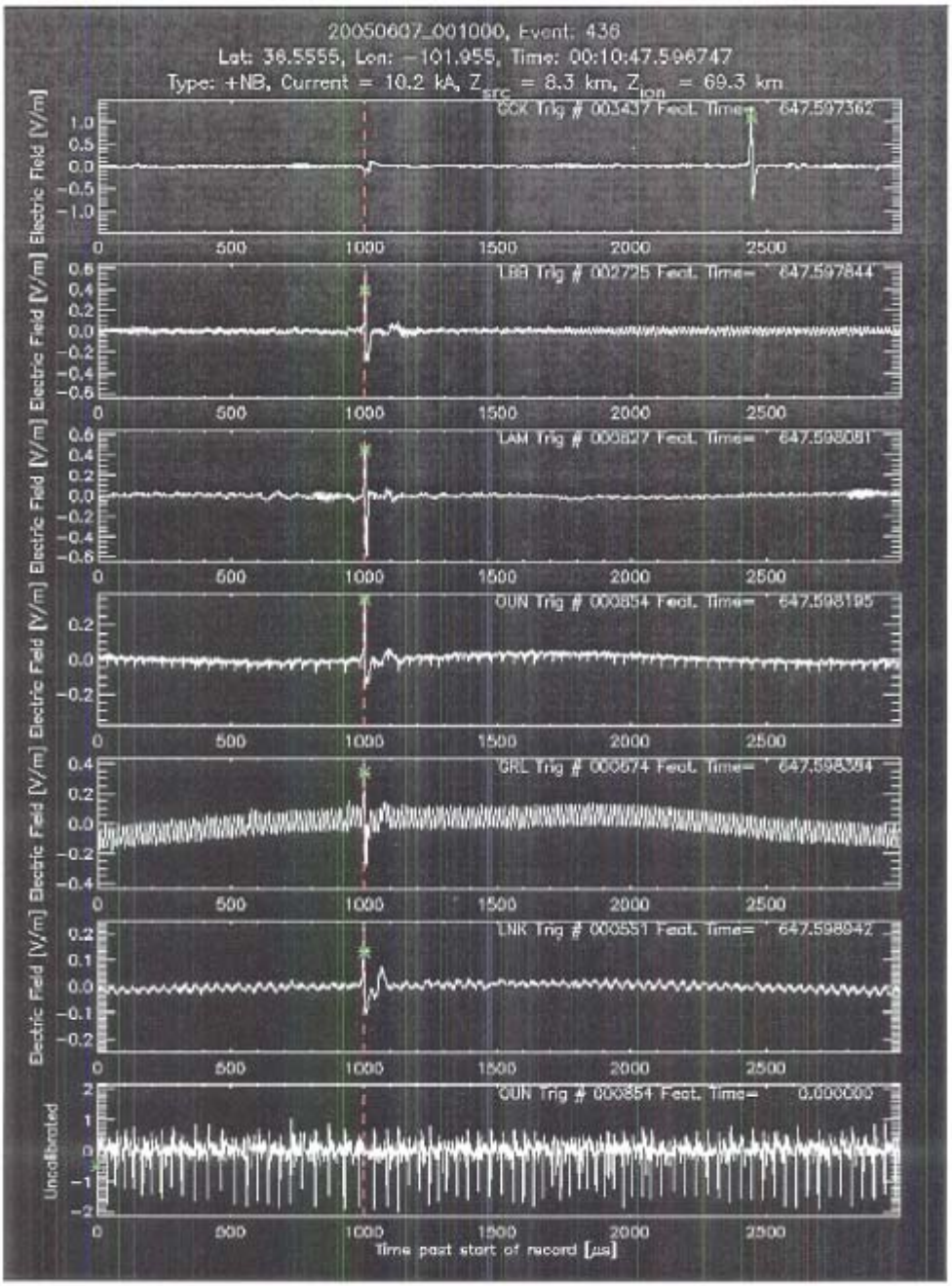

Figure 3.2: An example of the waveform patterns obtained from all 6 LASA sensors for a given NBE+ occurrence with source height 8.3 km. Note the extremely noisy trigger data from the GRL station. Bottom panel is uncalibrated data and should be ignored. (From LANL; courtesy of Tim Hamlin)

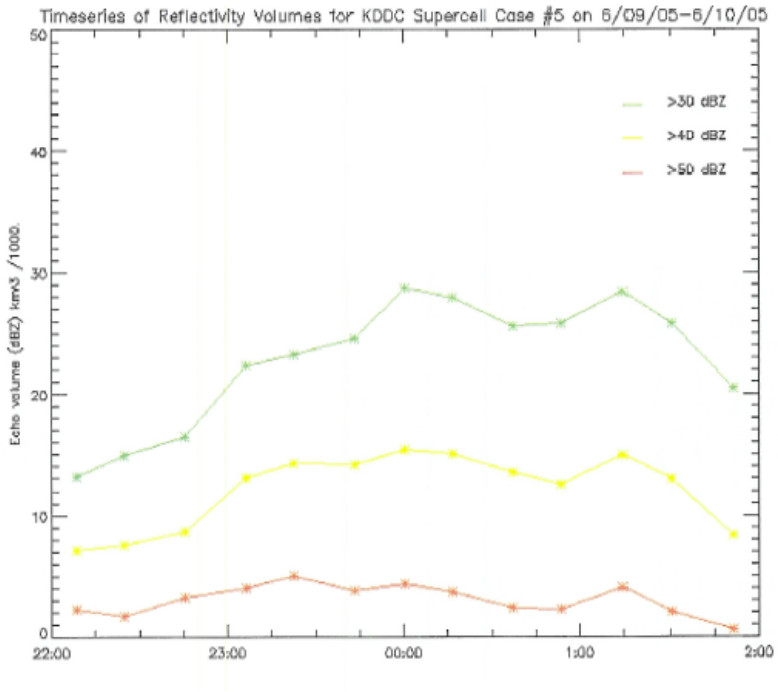

Figure 3.3: Example of Echo Volume Profiles for select storm at 30, 40 and 50 dBZ. Note that in future analyses only the 50 dBZ values were used.

3.7 SPC Reanalysis: CAPE and Shear Profiles

The final analysis step was to look at the CAPE and shear profiles of each storm and note if any trend resulted, in terms of the mesoscale environmental conditions being connected to NBE+ frequency. To accomplish this task CAPE and 0-6 km shear profiles were obtained from the Storm Prediction Center's online archive of Reanalysis products. While numerous other dynamic parameters were expressed, it was chosen to use these two as gross estimations of the storm environment. The calculations of CAPE and Shear were done using sounding data taken from locations as close to the storm both in time and range. While not all soundings were made directly within the storm or at the exact moment of storm intensification, the general environmental conditions present were captured. The possible dynamical connections between these parameters and NBE occurrence will be discussed further in the Results section.

Chapter 4

RESULTS

4.1 Bow Echo Results

Five Bow Echo cases were identified within the LASA Network during May-June 2005. Specifically, the lightning characteristics of two individual cell bow echoes and three squall-line bow echoes were collected and analyzed every 15-min, in conjunction with 50 dBZ Echo Volume (EV), and NEXRAD Radar Plan Position Indicator (PPI) images. The National Lightning Detection Network was employed to collect all Cloud-to-Ground lightning (CG) data, while LASA was used to collect Intra-Cloud Flash data (IC), and positive Narrow Bipolar Event (+NBE) data. Note that for the squall-line bow echo cases, several individual cells within the overall line were also examined using a similar procedure.

The 50 dBZ Echo Volume is used as a quantitative measurement for overall storm strength. The lightning statistics are linked to the relative changes seen in the Echo Volume profiles, whereby specific lightning types (IC/CG-/CG+/+NBE) and parameters will be used as proxies for storm strength. Lastly, the PPI Radar images provide a subjective confirmation of the physical bowing of the storm to support the subjective bow index being used. General storm intensification/weakening will also be verified using these PPI images. For the individual cell cases, the 50 dBZ Echo Volumes are compared

to the EV of the overall bow echo to determine the cell's behavior relative to the overall storm.

4.1.1 Bow Echo Case #1: Individual Cell Bow, 7 June 2005.

At 0:00Z on 7 June an intense convective cell developed approximately 200 km southwest of the Fredrick, Oklahoma NEXRAD (KFDR) site along the Texas/Oklahoma border. It proceeded to track northeast over the next 45 minutes and grow slightly in intensity. Seen in Figure 4.1, a relative increase in IC lightning coupled with a slight drop in CG- lead to a higher IC/CG ratio over this timeframe, suggesting strengthening. The findings of Boccippio (2002) linked increasing IC/CG lightning ratios with storm intensification. At 0:45Z, the individual cell merged with other convection and remained indistinguishable until 3:15Z. From 3:15Z-4:45Z, the individual cell rapidly intensified, as denoted in Figure 4.1 by a steady increase in the 50 dBZ Echo Volume. Increases in IC, CG-, and CG+ (total lightning) support this observation in agreement with Lang and Rutledge (2002). Intra-cloud lightning rates peaked at around 60/min, while CG+ frequency topped out at ~ 0.6/min. Note that the NBE+ profile exhibited no observable trend over this time period. Additionally, the cell began to quickly bow outward, as shown in Appendix Figure A.1. At 4:45Z, all lightning parameters decreased, just prior to the point of maximum storm bowing, which occured at 5:00Z. The 50 dBZ Echo Volume (EV) dropped slightly at 4:45Z, denoting a slight weakening. Shortly after the bow peak, the EV began to increase once again. IC/CG-/CG+ parameters increased as well. There was no observable trend in the +NBE profile. This secondary strengthening lasted from 5:00Z-6:15Z. The cell became completely linear over this time period (Fig. A.2). Interestingly, this intensification preceded a second bowing phase, which started at

6:15Z, peaking at 7:00Z (Fig. A.3). From 6:15Z onward, the 50 dBZ EV continually decreased, as well as all lightning parameters, including NBE+'s. The majority of +NBE's occurred on the two flanks of the cell, concurrent with the apparent location of the bookend vortices (Fig. A.4). Negative NBE's (-NBE) were not plotted for this or any other case, due to the fact that the majority of Narrow Bipolar Events (80%) are +NBE's (Wiens et al. 2008).

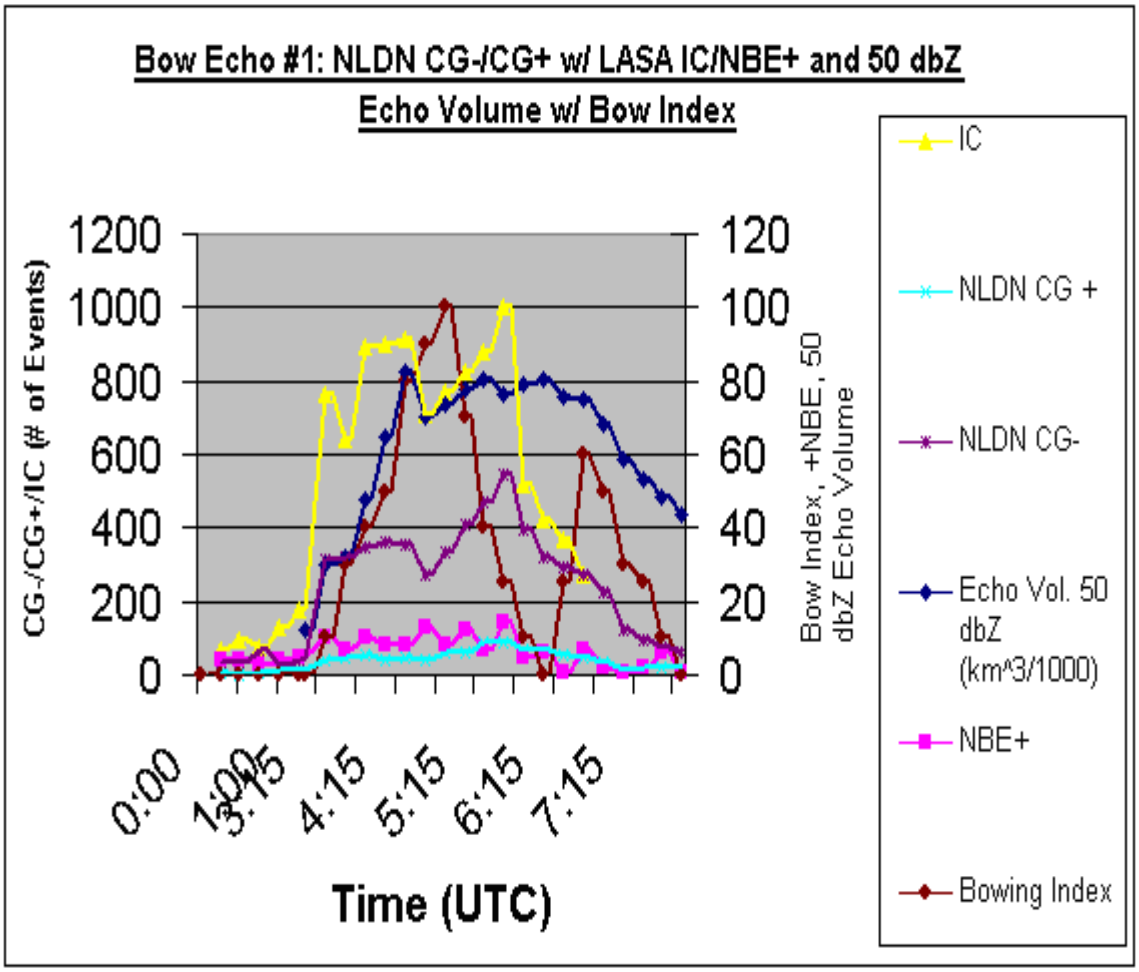

Figure 4.1: Lightning and Echo Volume Characteristics of Individual/Convective Cell Bow on 7 June 2005 near Fredrick, OK from 0:00Z-8:00Z. Left Y-axis is plotting CG-, CG+ and IC lightning. Right Y-axis is plotting 50 dBZ EV (with units expressed), NBE+ and Bow Index on a unit-less scale of 1-100. NBE+ profile is ragged and agrees only sporadically with lightning parameters.

4.1.2 Bow Echo Case #2: Squall-Line Bow Echo, 1 June 2005.

At 05:30Z on 1 June 2005, a linear squall line associated with a frontal passage was draped over a large portion of North Central Texas. Extending some 200 km, the convective line proceeded to push southeast towards the Texas Gulf Coast over the next 5-6 hours. The NEXRAD site KDYX (Dyess AFB, TX) was used to monitor the storm from 5:30Z-8:00Z, while KEWX (Austin/San Antonio, TX) served to track the time period from 8:00Z-11:00Z. It should be noted that for this bow echo case, lightning data will be analyzed not only for the overall bow, but also for three select individual cells within the larger scale bow. The lightning characteristics of the entire squall-line bow are presented in Figure 4.2. From 5:30Z-6:45Z, the storm bowed outward and reached its bow maximum at 6:45Z (Fig. A.5). Over this same time frame, the 50 dBZ Echo Volume (EV) decreased, likely signifying a weakening of the storm intensity. The CG-/CG+ lightning increased in concert with decreasing IC flash rates, resulting in a lower IC/CG ratio which can also be an indicator of storm weakening (Boccippio 2002). Radar PPI's images of the storm at the two end timepoints show this trend (see Fig. A.5). The NBE+ profile exhibited no definitive trend over this time period. Note that the IC parameter is exceptionally low relative to the amount of total CG, due to the 43.8% detection efficiency of LASA-based IC, relative to the 90% detection efficiency of NLDN CG strikes (Wiens et al. 2008, Cummins et al. 1998). This problem is further exacerbated by the bow echoes' location at the edge of the LASA Network. Regardless of location within the network, this issue is substantial and therefore the values for IC and IC/CG should not be taken as truth, but used only in a relative sense. From 6:45Z-8:00Z the line became more linear (Fig. A.6). Concurrently, the 50 dBZ EV increased and maximized at 8:00Z.

The CG-/CG+/IC time series show the same profile. Although the trend is not as smooth, NBE+ also peaked at 8:00Z. Here the +NBE appears to serve as an additional proxy for storm intensification (Wiens et al. 2008). This maxima in storm intensity preceded a second bowing cycle which lasted from approximately 8:00Z-10:00Z. From 8:00Z-9:00Z, CG-/CG+ and IC all decreased along with a decreasing 50 dBZ EV. A radar image of the storm at 9:00Z can be compared to the 8:00Z image to show a weakening bow (Fig A.7). At 9:15Z, the bow index dropped slightly then began to increase again until 10:00Z. Interestingly, just prior to 9:15Z, a small maximum occurred in the 50 dBZ EV and IC/CG-/CG+ parameters. While this feature preceded an increase in the degree of bowing, similar to what was observed at 8:00Z, the relative change of these parameters was not large enough to conclude a strong relationship. Regardless, the bow index maximized at 10:00Z (Fig. A.8). After 10:00Z the storm became more linear and weakened, supported by the steady decrease of total lightning (IC/CG-/CG+) (Lang and Rutledge 2002). Note that overall, the NBE+ profile was essentially flat, with NBE+'s only being applicable to the trends of the traditional lightning parameters between 6:45Z and 9:15Z. Here NBE+ rates maximized at approximately 2/min, in agreement with rates previously seen (Wiens et al. 2008).

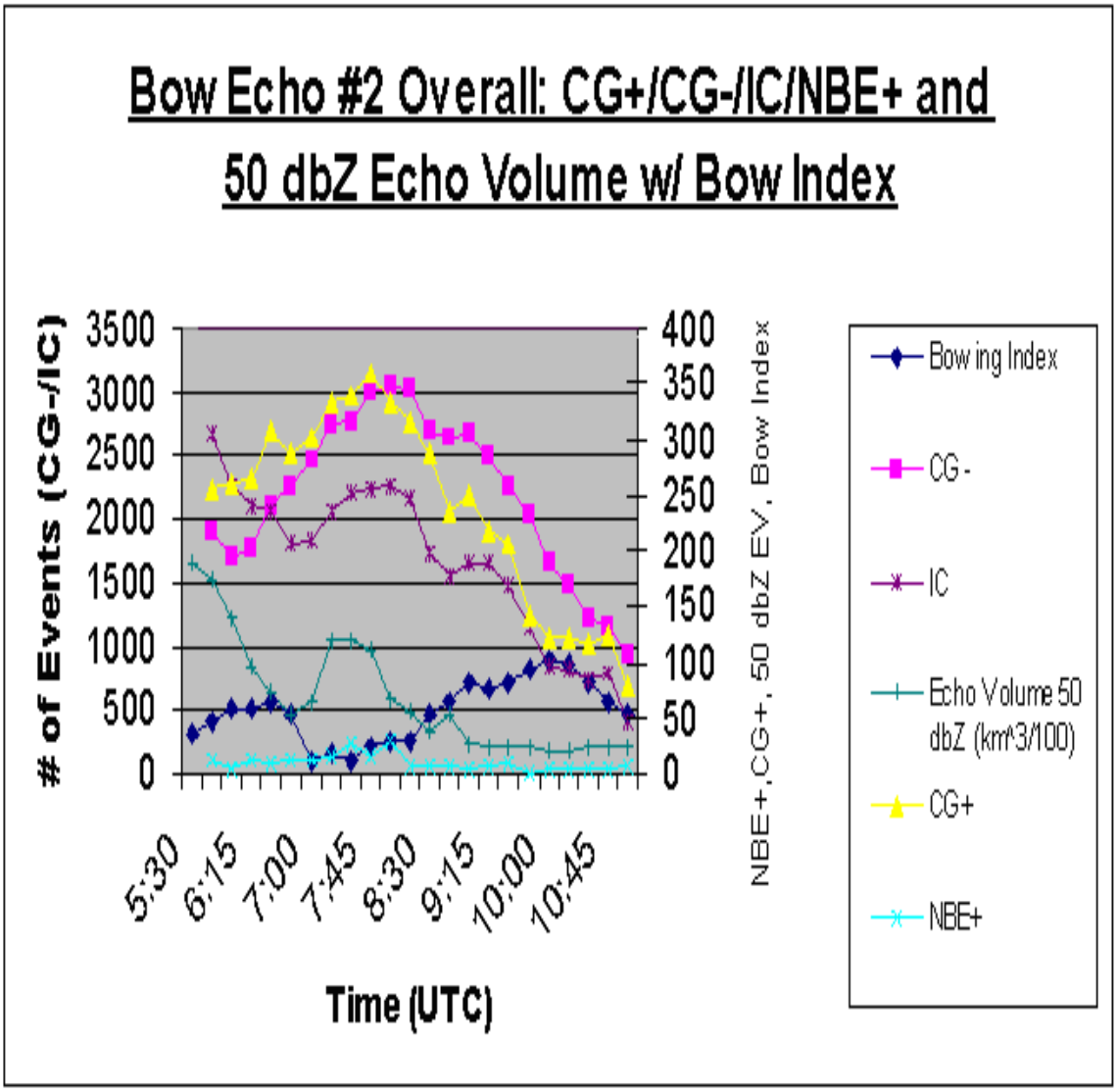

Figure 4.2: Lightning and Echo Volume Characteristics of Squall-Line Bow on 1 June 2005 in North Central Texas, from 5:30Z-11:00Z. Left Y-axis is plotting CG- and IC only. The Right Y-axis is plotting NBE+,CG+, 50 dBZ EV, and Bow Index on scale of 1-100.

4.1.2.1 Preface for Analyzing Individual Cells Within the Overall Bow Echo

The primary goal in observing this individual cell, and others to follow, will be to assess if these cellular lightning characteristics are correlated to, or indicative of, the physical bowing of the overall storm. Additionally, it will be important to determine the degree to which the individual cell influences both the convective strength and the

electrical characteristics of the overall storm. As a meso-scale feature present within the larger convective line, it will be key to note if these independent entities react in concert with the changes seen in the overall line, or if they do not. Specifically, the influence of the individual cell towards positive narrow bipolar events (+NBE's) will be postulated. Furthermore, while not all cellular components within each overall bow echo will be analyzed, multiple cells were chosen from different portions of the overall storm. Offering a degree of random variability, this portion of the study will lend support towards determining if these individual cells are largely consistent in their behavior.

4.1.2.2 Individual Cell #1 Located Within Bow Echo #2 from 5:30Z-9:15Z

Located on the southwest end of the overall squall-line, an individual pocket of strong convection was tracked for nearly four hours over central Texas. Note in Fig. 4.3, that IC lightning was not used, for reasons discussed previously. Also, no 50 dBZ Echo Volume (EV) profile existed after 6:30Z for the cell only. From this time-point on, low level (0.5 degree) Radar PPI images were used to infer storm intensity. Initially, the overall storm 50 dBZ profile decreased from 5:30Z-6:30Z. Over this same time the bow index of the parent line increased, with a bow maximum occurring just prior to 6:45Z (Fig A.9). In comparison, the cell behaved quite differently over this time span, actually increasing in intensity between 6:00Z and 6:30Z, as seen in the 50 dBZ EV. Increases in CG- and CG+ accompanied the increase in EV. After 6:30Z, CG- and CG+ continued to increase, peaking at approx 7:00Z. NBE+ frequency also peaked at this time. While increasing CG lightning rate, nor NBE+ rates of such low frequency may not directly confirm cell strengthening/weakening, PPI radar images at 6:30Z and 7:00Z of the cell were used to confirm a continued strengthening (Fig A.10 and A.11). Note that the cell

has expanded in area. These increases in CG- and CG+ contributed to the overall profile, as approximately 20% of the CG- and CG+ strikes were assigned to this cell alone. The overall storm was also experiencing increasing CG frequency over this time frame, though coupled with a decreasing IC frequency. In terms of the NBE+, the overall profile appears somewhat random, when it should have been decreasing over this timeframe. This assumption follows from the research of Wiens et al. (2008), whereby a weakening storm should statistically produce fewer +NBE's. Though only a few +NBE's came directly from this cell, the overall trend was influenced by this cell. From 7:00Z-7:30Z the CG- and CG+ parameters of the cell quickly fell, as well as NBE+ values. PPI images of the cell however, were not able to confirm a weakening or strengthening (Fig. A.12). Overall, the storm continued to intensify based on 50 dBZ EV until 7:15Z. The cloud-to-ground lightning and +NBE trends for the overall bow echo over this timeframe, did not appear to be adversely influenced by the cellular lightning characteristics. From 7:30Z-8:00Z, cloud-to-ground lightning in the cell rebounded up to their previous frequencies, with little change in +NBE frequency. The cellular lightning characteristics acted in concert with the increasing cloud-to-ground lightning frequency of the overall bow over this time span. Radar images at 7:30Z and 8:00Z exhibit an apparent weakening of the cell (Fig. A.13). The storm overall during this same timeframe also weakened and continued to do so until 9:30Z, with the exception of a small intensification from 8:30Z-8:45Z. From 8:00Z on, the cell weakened as shown by radar PPI at 8:45Z and 9:30Z, respectively (Fig. A.14 and Fig. A.15). The individual cell from 8:30Z-8:45Z did not experience any increases in CG lightning or +NBE's. It is important to note that +NBE profiles employing rates < 0.5 per minute, should not be trusted as uncertainty of the

measurement may influence the overall trend. It does not appear that the physical bowing of the storm is connected to the relative strengthening of this individual cell. The overall +NBE trend was affected by the behavior of this individual cell. The lightning characteristics of this individual cell served to enhance those features already present in the overall storm lightning profile. The lightning flash rate within this cell was such that it did not constitute a majority of the overall flash rate for the storm at any one time point. Therefore, changes in the individual cell flash rate were not reflected in the overall storm lightning profile.

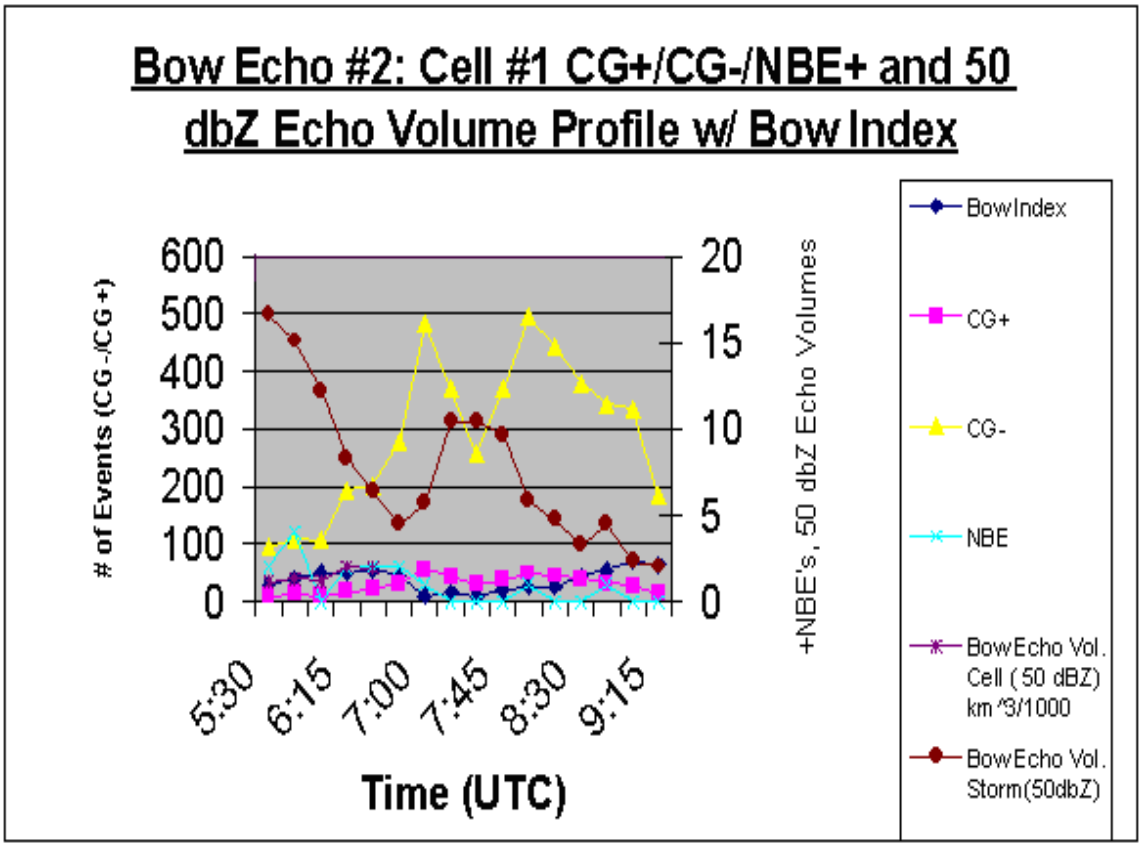

Figure 4.3: Lightning and EV Characteristics for Individual Cell #1 found within Bow Echo #2 on 1 June 2005 from 5:30Z-9:45Z. The Left Y-axis is plotting CG- and CG+ and bow index on a unitless scale of 1-100. The Right Y-axis is plotting +NBE's, and the EV's of both cell and overall storm (units listed).

4.1.2.3 Cell #2 Located Within Bow Echo #2 from 5:30Z-8:30Z.

From 5:30Z-8:30Z, a second individual cell located in the central portion of the overall bow was followed, and the following lightning characteristics were obtained relative to the overall storm. Denoted in Figure 4.4, from 5:30Z-6:30Z, both the storm and cell weakened as seen by their 50 dBZ EV decreases, and are supported by radar PPI images for these timepoints (Fig. A.16 and Fig. A.17). The decreasing CG frequency seen in the cell did not strongly influence the lightning activity in the overall line. From 6:30Z-6:45Z, while the storm showed continued weakening, the cell intensified as supported by jumps in all lightning parameters and the 50 dBZ Echo Volume (EV). The cloud-to-ground lightning characteristics of both cell and storm matched over this time frame. The bow echo maximum of the parent line occured at 6:45Z as well (Fig A.18). Following this sharp rise, the CG- and CG+ parameters slowly declined, and the 50 dbZ Echo Volume reflected a slow weakening, from approximately 7:00Z-8:30Z. Meanwhile, the storm rapidly intensified from 7:00Z-7:30Z as denoted by the 50 dBZ EV, then lost strength from 7:30Z-8:30Z (Fig. A.19 and Fig A.20). While the majority of the time found agreement between the convective strength/lightning profiles of the cell and overall storm, in both cell #1 and cell #2, the convective strength and CG lightning maximized prior to the overall storms peak in both of these parameters. During this period of disagreement, the overall bow echo CG lightning did not appear to be substantially influenced by the cellular lightning characteristics. Note, that the NBE+ characteristics of the cell are poorly related to the other lightning parameters at the 7:30Z timepoint. This certainly affected the overall +NBE trend at this point. It does not appear that the physical bowing of the storm enhanced the lightning characteristics of the cell.

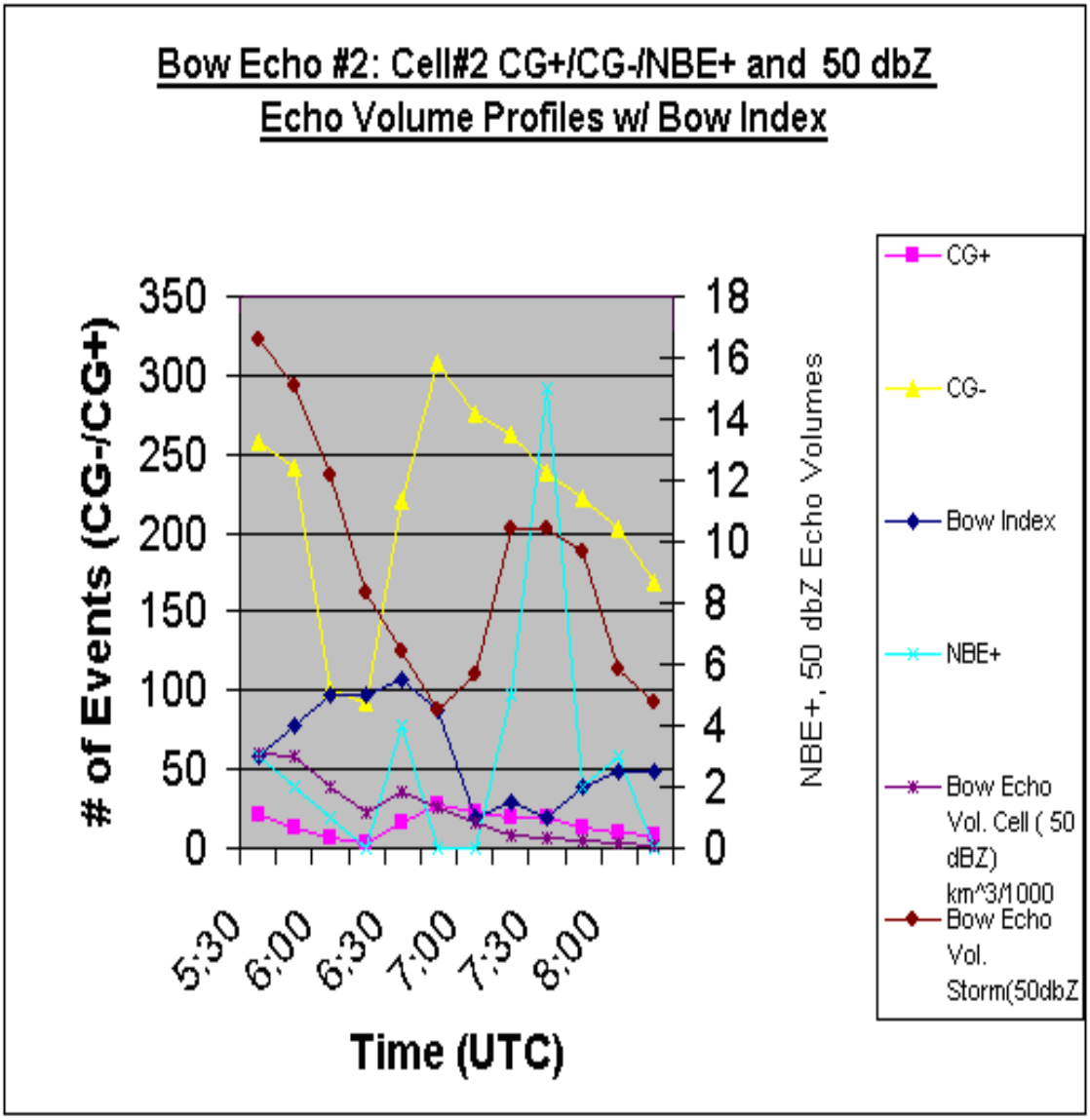

Figure 4.4: Lightning and Echo Volume Characteristics for Cell #2 found within Bow Echo #2 over northeast Texas on 1 June 2005 from 5:30Z-8:30Z. The Left Y-axis is plotting CG-/CG+ and the bow index on a unitless scale of 1-100. The Right Y-axis is plotting both Echo Volumes (units listed) and NBE+ number.

4.1.2.4 Cell #3 Located Within Bow Echo #2 on 1 June 2005.

A third individual cell occurring just east of Cell #1 was tracked from 6:45Z-9:30Z over Southern Texas. The behavior of this cell was markedly different than the first cell noted. Overall, this cell exhibited a strong likeness to the convective strength pattern of the overall storm. As seen in Figure 4.5, from 6:45Z-7:45Z, both storm and cell grew in convective strength as denoted by their respective 50 dBZ Echo Volume profiles. All lightning parameters were consistent with this intensification as well. The spike seen in the +NBE profile for the individual cell is a large contributor towards the maximum +NBE point seen in the overall storm profile. In contrast to the first two cases, the cell #3's convective strength peaked after the overall storms' convective strength at 8:00Z. It does not appear that the lightning generated from this cell, markedly altered the overall storm lightning CG-/CG+ and IC lightning profiles. From 8:00Z-9:30Z, both cell and storm generally weakened, as reflected in their EV profiles. As expected, the peak of storm convective strength precluded the maximum bow index of the storm.

In summation, the three individual cells were shown to have marked impacts on the +NBE profile of the overall storm. Meanwhile, the cellular lightning characteristics, and cell convective strengths appeared to match and/or slightly lag the overall storm profiles for these parameters a majority of the time. During these time frames, the cells were shown to contribute to the overall storm lightning characteristics, but individually did not possess a high enough lightning flash rate to constitute a majority of the overall lightning. Therefore, their ability to directly control the overall lightning profile is not supported. Where there are periods of disagreement, the lightning frequencies of the

overall convective line appeared to be high enough in frequency to mask the opposed lightning characteristics of the individual cell.

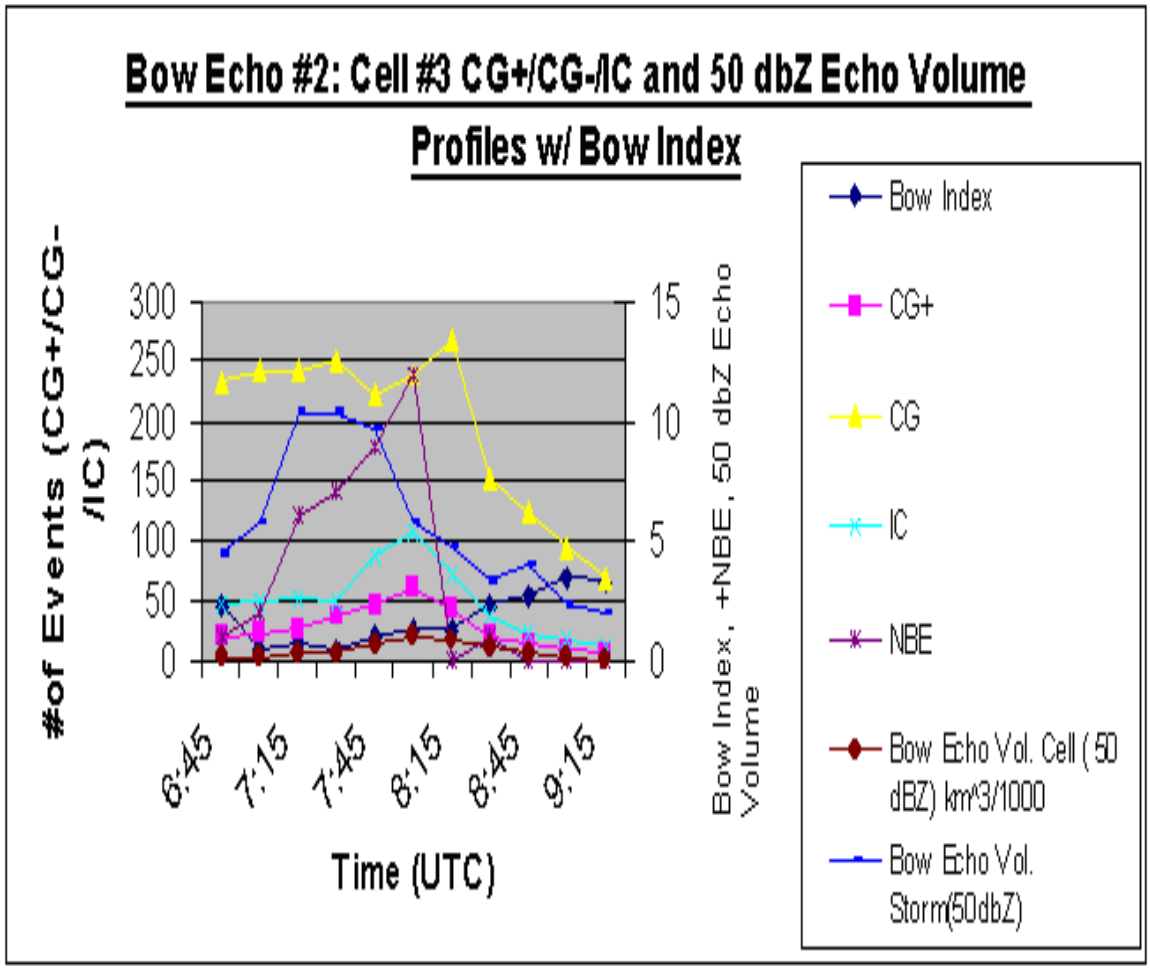

Figure 4.5: Lightning and Echo Volume Characteristics for Cell #3 found within Bow Echo #2 on 1 June from 6:45Z-9:30Z. The left Y-axis is plotting CG+/CG-/IC and Bow Index on a 1-100 unitless scale. The right Y-axis is plotting NBE+ and both Echo Volumes (units shown).

4.1.3 Bow Echo Case #3: Individual Cell Bow on 7 May 2005.

On 7 May 2005, a small isolated area of convection rapidly intensified west of Dodge City, Kansas (KDDC), leading to a short period of outward bowing, followed by a rapid weakening. Although short-lived, this event exhibited lightning and convective strength characteristics similar to prior cases. Note that IC and CG lightning events were combined due to an exceptionally low IC return for this bow echo. This formed a total lightning parameter. This parameter was previously employed by Lang and Rutledge (LR) (2002) to estimate storm strength. A possible explanation for this low IC rate could be that the LASA network was not fully operational on this date (personal correspondence, K. Wiens). As seen in Figure 4.6, the timeframe of 6:45Z-7:15Z shows that the storm was at a steady state. Total Lightning and CG- remained steady with CG+ lightning decreasing. Radar PPI images from 6:45Z and 7:15Z support this steady state (Fig. A.21 and Fig. A.22). The storm bowed only slightly during this time. A rapid intensification then occurred from 7:15Z-7:45Z as indicated by the 50 dBZ Echo Volume (EV) plot. CG+ and Total Lightning increased as well. The bow index also sharply increased, maximizing at 8:00Z (Fig A.23), just after the peak of storm convective strength. From 7:45Z-9:15Z the 50 dBZ EV decreased as did Total Lightning. The bow echo quickly returned to a linear state by 8:45Z (Fig. A.24). While Jacobsen and Heavner (2005), concluded that NBE activity can be correlated to storm convective strength, the NBE+, as a proxy for storm strength, should not be used in this case given its very low frequency.

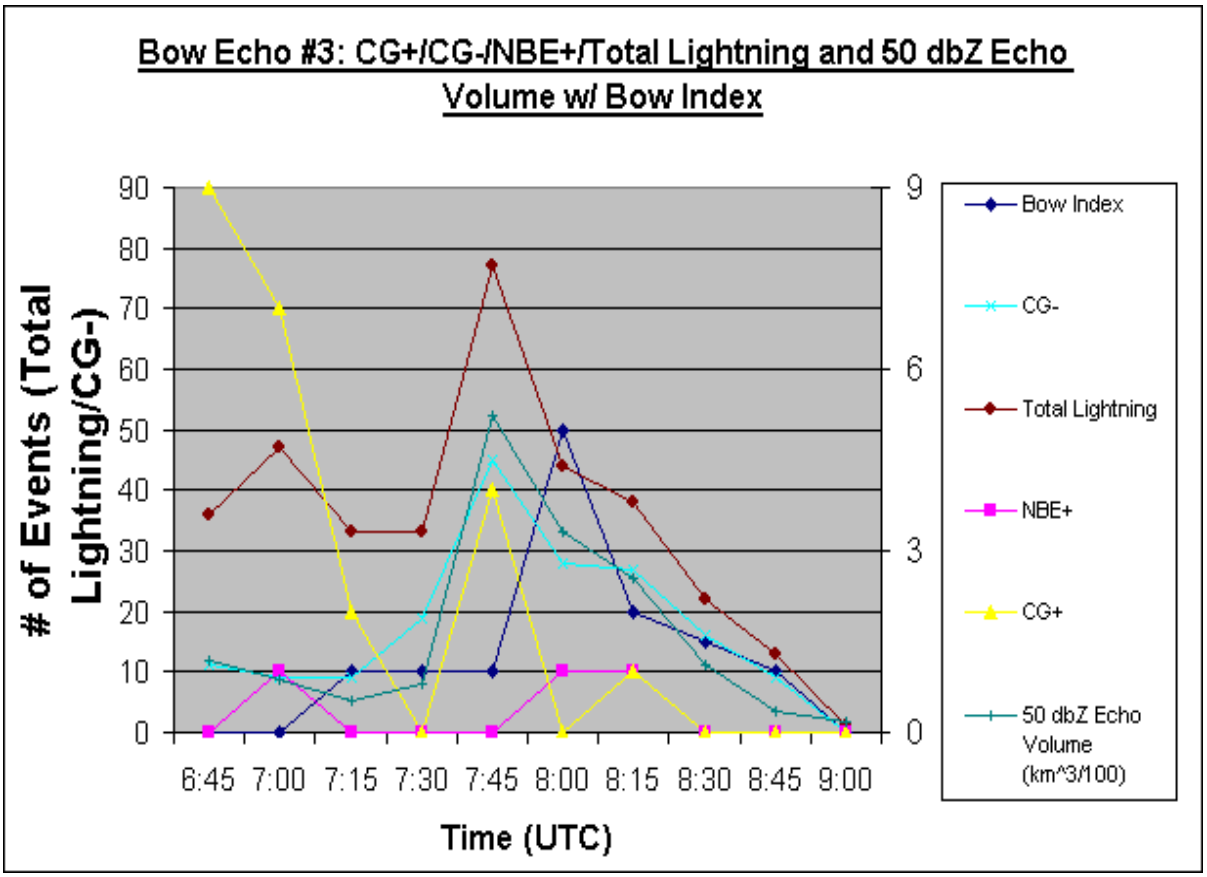

Figure 4.6: Lightning and Echo Volume Characteristics for Bow Echo Case #3 on 7 May 2005 from 6:45Z-9:00Z. The left Y-axis is plotting Total Lightning, CG- and the bow index (unitless) on a scale of 1-100. The right Y-axis is plotting CG+,NBE+ and 50 dbZ Echo Volume.

4.1.4 Bow Echo Case #4: Squall-Line Bow on 13 May 2005.

On 13 May 2005 at 3:15Z, a squall-line approximately 100 km in length began to show signs of bowing as the line progressed east-north-east over western Oklahoma and the Texas Panhandle. The KFDR (Fredrick, OK) NEXRAD was used to gather the necessary radar images. From 3:15Z-5:45Z the line bowed twice, such that there was a small maximum in the bow echo index at 3:45Z followed by a slight linearization. From 4:00-5:45 the storm began to bow again, attaining a maximum bowed configuration by 5:45Z (Fig. A.25). Prior to each of these bow maximums, maximums in the lightning data

parameters (IC/CG+/CG-) were observed, as seen in Figure 4.7. Based on Total Lightning measurements this would suggest a convective strength peak at these two points (LR 2002). The slight decrease in bow angle from 3:45Z- 4:00Z was reflected by the relative decrease in IC lightning relative to CG at this point; lower IC/CG (Boccippio 2002). Note that the 50 dBZ Echo Volume only showed a slow strengthening up to the 4:15Z time, leading the second bow peak. This was followed by a slow weakening in convective strength based on a slowly decreasing EV, from 4:15Z-7:00Z,. It would appear that the small perturbation in bow index was not manifested in the 50 dBZ Echo Volume at 3:30-3:45Z, in contrast to the lightning data. Radar PPI images at 3:30Z and 3:45Z show no visible strength change. (Fig A.26 and Fig.A.27). Of note, the increasing CG- parameter from 5:30-6:00Z, does not suggest strengthening, but rather is coupled with decreasing IC, denoting a weakening pattern. Furthermore, the lack of NBE+ in this bow echo is a curious result. There are only 3 NBE+ discharges over the entire duration.

4.1.4.1 Individual Cell #1 located within Bow Echo #4 on 13 May 2005

A strong area of convection present on the southwest flank of the overall bow echo was tracked for approximately 2.5 hours until the cell completely separated, and became independent of, the convective line. Over this time frame, the overall bow echo exhibited a slow strengthening, leading to an intensity maximum at 4:15Z, followed by a slow weakening phase (Figure 4.8). As seen in the previous cases, the bow peak was delayed from the actual convective strength peak of the overall line, with the bow maximum of the complete storm occurring at 5:15Z, In terms of the individual cell, the trends obtained agree nicely with those seen in the overall storm. From 3:45Z-4:15Z, the 50 dbZ Cell EV increased, in line with the overall storm EV.

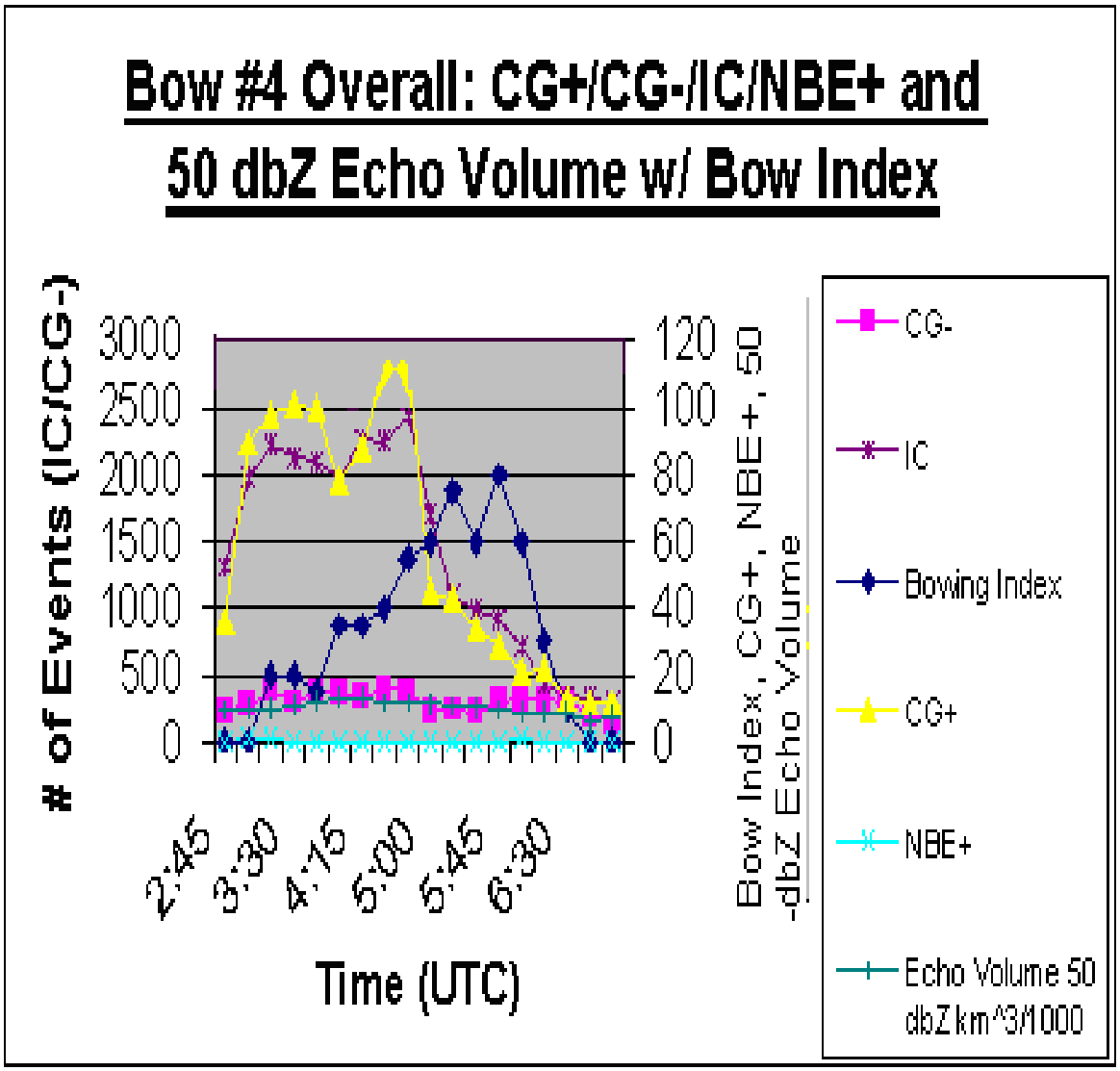

Figure 4.7: Lightning and Echo Volume Characteristics for Bow Echo Case #4 Overall on 13 May 2005 from 2:45Z-7:15Z. The left Y-axis is plotting IC and CG- only. The right Y-axis is plotting NBE+, CG+, 50 dbZ Echo Volume (units seen), and bowing index (unitless) on a scale of 1-100.

A relative decrease in CG- versus IC coincided with this intensification. Research from Boccippio (2002) concluded that an increasing IC/CG ratio was indicative of a strengthening storm. From 4:15Z-4:45Z, the CG- quickly increased producing a much lower IC/CG ratio. Coupled with a decreasing CG+ rate, this suggested a weakening cell,

a feature noted in prior research (Williams 2001). This trend was confirmed by a decreasing 50 dBZ cell EV and Radar PPI images from 4:15Z and 4:45Z (Fig. A.28 and Fig. A.29). The storm also weakened from 4:15Z-4:45Z, based on a decreased storm 50 dBZ EV. Overall, the cell does not appear to be influenced by the bowing of storm, and acted similarly to the overall storm both in terms of its' convective strength and associated lightning characteristics. Over small portions of the storm lifecycle (3:00-3:45Z and 4:45Z-5:00Z), the cell did act opposite to the overall storm. It is apparent that from 4:45-5:00Z this cell was not able to affect the overall storm EV, however the cell lightning perturbations were strongly reflected in the overall storm lightning profiles. There are basically no +NBE's in this cell despite the relative intensity of both storm and cell.

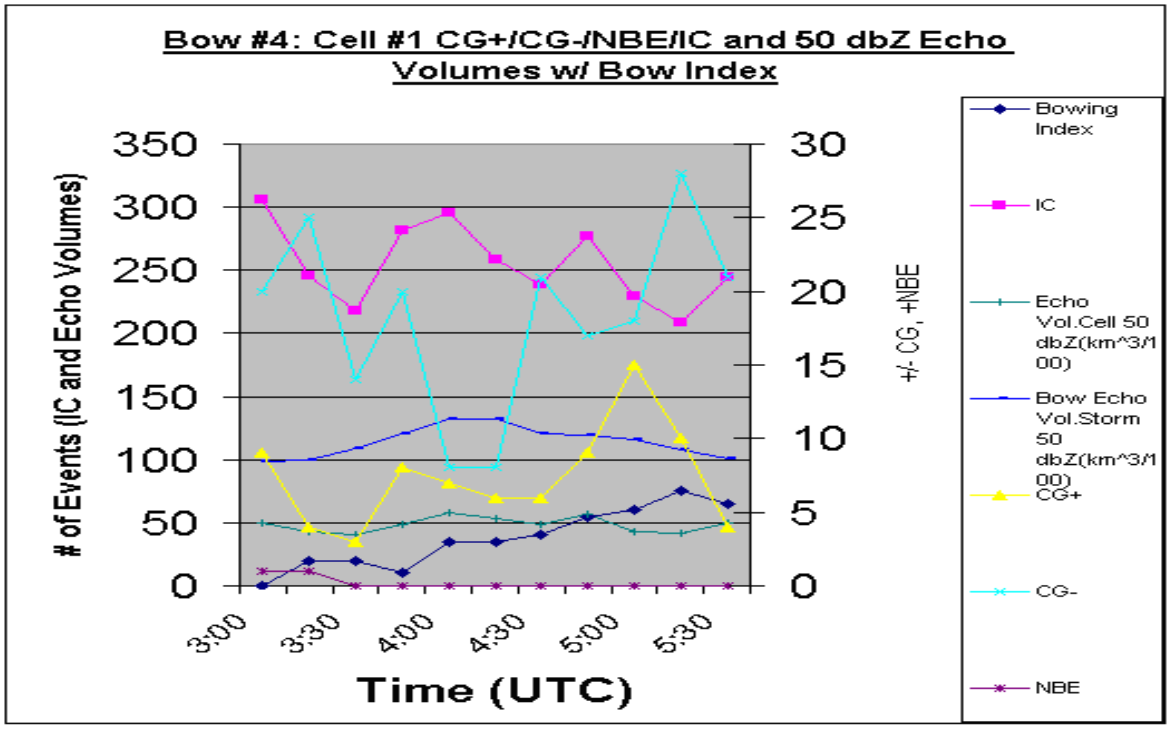

Figure 4.8 Individual Cell #1 and Bow Echo #4 on 13 May 2005 from 3:15Z-5:45Z. The left Y-axis is plotting IC , both 50 dBZ Echo Volumes (note units included), and the bow index on a scale of 1-100. The right Y-axis is plotting CG+/CG- and NBE+.

4.1.4.2 Individual Cell #2 Located Within Bow Echo #4 on 13 May 2005.

As viewed in Figure 4.9, at 3:45Z, an intense cell imbedded in the southwest portion of the squall-line began to rapidly strengthen, reaching a convective strength maximum based on 50 dBZ Echo Volume at 4:30Z. This intensity maximum was further supported by a sharp increase in IC lightning coupled with a drop in total CG at this time. Past research has shown that an increasing IC/CG denotes strengthening (Boccippio 2002). At 5:30Z-5:45Z, the cell experienced another small period of strengthening, reflected in an increasing IC/CG ratio (Boccippio 2002). This observation is further supported by radar PPI cell images at 5:30Z vs. 5:45Z (Fig. A.30 and Fig. A.31). In comparison to the storm as a whole, both storm and cell experienced convective strength peaks at 4:30Z and both exhibited slow declines afterwards with the exception of the cells slight intensification period at 5:30Z. In contrast to Cell #1 of this case, the cell lightning frequencies at 5:30Z were not strongly reflected in the overall storm lightning characteristics or overall storm EV. This perturbation at 5:30Z was likely a more unique occurrence across the storm as a whole. There are no +NBE's in this cell. Both cells do not appear to be influenced by the bowing of the storm itself.

4.1.4.3 Cell #3 Found Within Bow Echo Case #4 on 13 May 2005

Located on the northeastern edge of the squall-line, this particular area of convection was located completely opposite the position of cells 1 and 2, yet the resultant cell profile remained consistent with previous findings. Therefore, this case will not be expounded upon but simply offered as further confirmation towards the consistent behavior in at least these three individual cell cases.

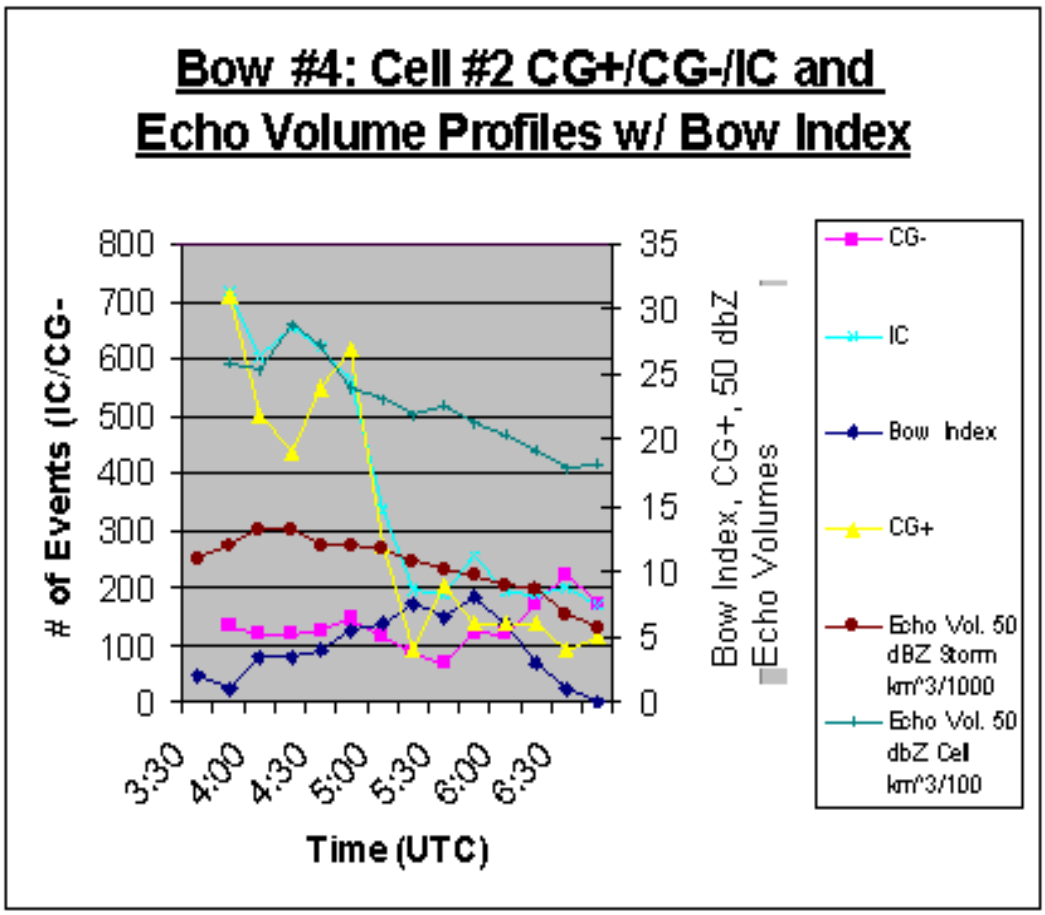

Figure 4.9: Lightning and Echo Volume Characteristics for Cell #2 found in Bow Echo #4 on 13 May 2005 from 3:45Z-7:00Z. Left Y-axis is plotting IC and CG-. Right Y-axis is plotting CG+, both 50 dBZ Echo Volume Profiles for storm and cell (units given), and the bow index on a unitless scale of 1-10.

4.1.5 Bow Echo Case #5: Squall-Line Type on 24 May 2005.

On 24 May 2005, a large but relatively isolated area of North/South oriented convection, approximately 125 km in length intensified just west of Wichita, KS (KICT) and proceeded to track generally northeast. This storm was particularly long in duration, lasting nearly 12 hours. Over the analysis time period, from 6:30Z-12:00Z, the storm underwent two complete bowing cycles before finally dissipating. From 6:45Z-8:00Z, the squall-line returned to a linear state after having reached a prior bow index maximum. As

seen in Figure 4.10, the corresponding lightning characteristics suggest that from 6:45Z-7:15Z, the line was weakening, given the observed decreases in total lightning (Lang and Rutledge 2002). Radar PPI's at these two times confirmed this weakening (Fig. A.32 and Fig. A.33). From 7:15Z-8:00Z, IC lightning significantly increased relative to small increases in both CG- and CG+; leading to an increased IC/CG ratio, observed to denote storm strengthening (Boccippio 2002). Note that this system produced high CG+ rates on the order of nearly 30/min. Also, a spike in +NBE frequency occurred at this time. A Radar PPI of the storm overall at 8:00Z exhibits this intensification (Fig. A.34). A maximum convective strength occurred in the 50 dBZ Echo Volume leading the actual bow peak at 8:45Z. One should be aware, that the 40 dBZ reflectivity contour was used from 8:15Z onward, rather than 50 dBZ, due to the low amount of volume which resulted from the 50 dBZ calculation.

From 8:15Z to bow peak, the storm convective strength weakened considerably, reaching a minimum in the 40 dBZ Echo Volume at the bow maximum. Decreasing +NBE rates supported this quantitative measure. This feature relating storm strength to NBE rate was previously noted by Suszcynsky and Heavner (2005). A decrease in CG+ also indicated storm weakening, as supported by the findings of Lang and Rutledge (2002). From 8:45Z-10:15Z, the line underwent a second bowing cycle, whereby it first became more linear, than bowed again to a maximum. A signature pattern of the convective strength lagging the bow maximum can be seen in the 40 dBZ EV.

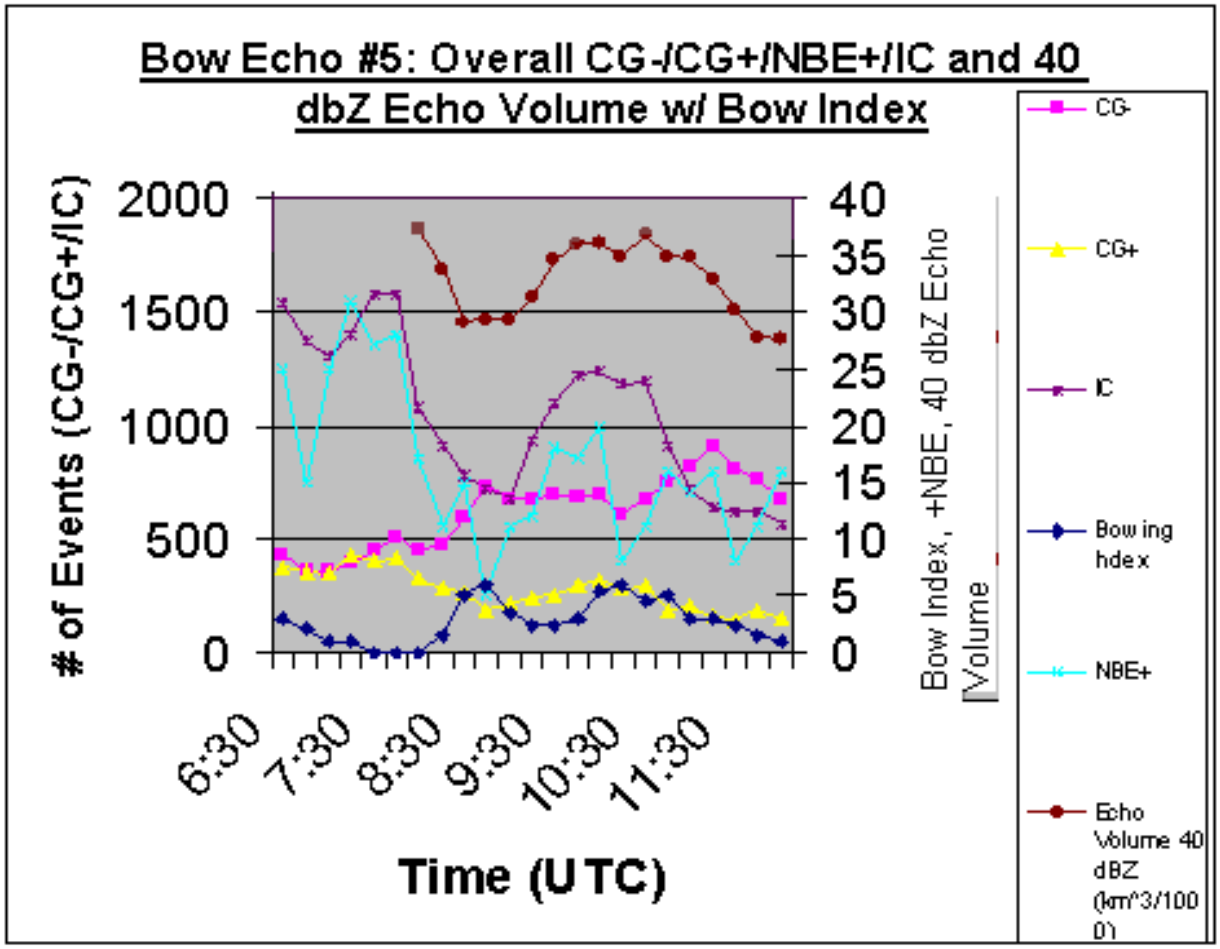

Figure 4.10: Lightning and 40 dbZ Echo Volume Characteristics for Bow Echo Case #5 on 24 May 2005 from 6:30Z-12:00Z. Left Y-axis is plotting CG-/CG+/IC. The Right Y-axis is plotting 40 dBZ EV, NBE+, and Bowing Index on a unitles scale of 1-10.

The lightning data produced a pattern similar to the first bow cycle and matches the EV tendency. Note that the NBE+ pattern generally follows the more traditional lightning parameters, however some anomalous spikes/dips are seen. It will be investigated whether these +NBE's are primarily generated from the individual cells or from the intervening echo between the various convective cells.

4.1.5.1 Cell #1 Located Within Bow Echo Case #5 on 24 May 2005

From 6:30Z-9:15Z a strong pocket of convection within the southern portion of the overall squall-line was monitored and both 50 dBZ Echo Volume and lightning data

was obtained for the cell. The overall storm complex weakened from 6:30Z-7:15Z as the bow index and 50 dBZ EV decreased. As seen in Figure 4.11, based on 50 dBZ EV, the storm began a modest intensification at 7:30Z, becoming more rapid at 8:15Z and eventually peaking at 8:45Z. The storm responded by producing a delayed physical bowing in its reflectivity pattern, which occurred at 9:00Z (Fig. A.35). An immediate decline in the bow index followed. Comparatively, the cell behavior was quite different. Where the overall storm weakened initially, the cell actually intensified from 6:30Z - 7:15Z, just prior to the onset of the overall squall-line intensification (Fig A.36 and Fig. A.37). This increase in both intra-cloud and cloud-to-ground lightning observed during this time frame in the cell was not reflected in the overall storm lightning trends. Less than 10% of the overall storm CG+ and approximately 25% of the overall storm CG- was generated from this cell alone. Conversely, though only 4 NBE's were registered from this cell at 7:15Z, this result contributed to the anomalous jump in +NBE's seen at this time. From 7:15Z-7:45Z the cell remained at steady state. At 7:45Z, the cell rapidly intensified and peaked in intensity at 8:15Z, denoted in the 50 dBZ EV Profile and Radar PPI image (Fig A.38). The lightning data supports the 50 dBZ cell EV maximum. Past research has linked sharp increases in total lightning (IC/CG-/CG+) with strengthening storms (Lang and Rutledge 2002). The increasing cell lightning characteristics were not reflected in the overall storm lightning profiles. Although, an anomalous spike in +NBE frequency occurred between 8:15Z-8:30Z, this particular cell did not markedly contribute to this feature, as only 1 +NBE was registered during this time-frame. Interestingly, the cell peak in 50 dBZ EV lead a similar storm convective strength peak that maximized 30 minutes later. A similar pattern in cell vs. storm convective strength was noted in two

cases prior for a different storm (see section 4.1.2.1 and 4.1.2.2. Where strong weakening was exhibited (8:45Z-9:15Z), a relative rise in CG- compared to a falling IC lightning parameter in the cell can be seen.

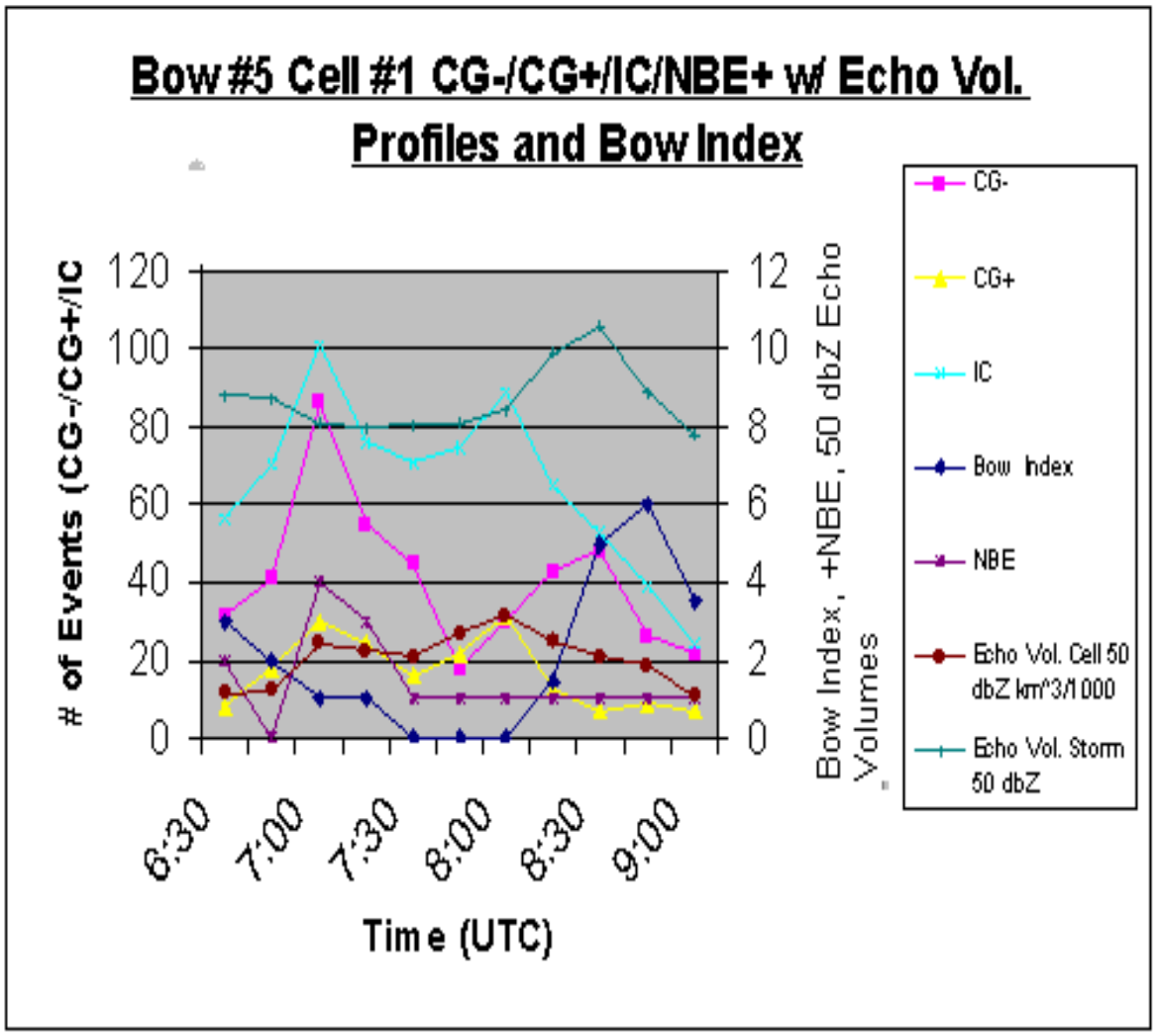

Figure 4.11: Lighting and Echo Volume Characteristics for Cell #1 within Bow Echo #5 on 24 May 2005 from 6:30Z-9:15Z. Left Y-axis is plotting CG-/CG+/IC. The Right Y-axis is plotting the EV's, NBE+'s, and Bow Index on a unitless 1-10 scale.

4.1.5.2 Cell #2 Found Within Bow Echo Case #5 on 24 May 2005.

Analyzed over nearly the same time period as Cell #1, this pocket of convection was found opposite Cell #1 on the northern end of the squall-line. These two cells actually match one another quite well. While a full graph interpretation will not be provided, it should be noted that the convective strengthening of the cell led the intensification of the overall storm, duplicating the previous cell case. The maximum in cell 50 dBZ (7:45Z) lagged the storm maximum 50 dBZ by approximately 45 min. The increasing cellular lightning frequencies from 7:15Z-7:45Z, support a similar trend seen in the overall storm from 7:15Z-7:45Z, with approximately 18% of the overall IC lightning and 20% of the CG- and CG+ lightning being generated from this cell alone. In terms of the +NBE, this cell has 6 +NBE's that occurred both at 7:30Z and 7:45Z. Constituting around 20 % of the overall storm +NBE total at this time point, the anomalous spike produced at 7:30Z is at least partially induced by this cell alone. Also, the small spike in +NBE for the cell at 8:30Z is also likely contributing to the +NBE spike seen in the overall storm profile at this point.

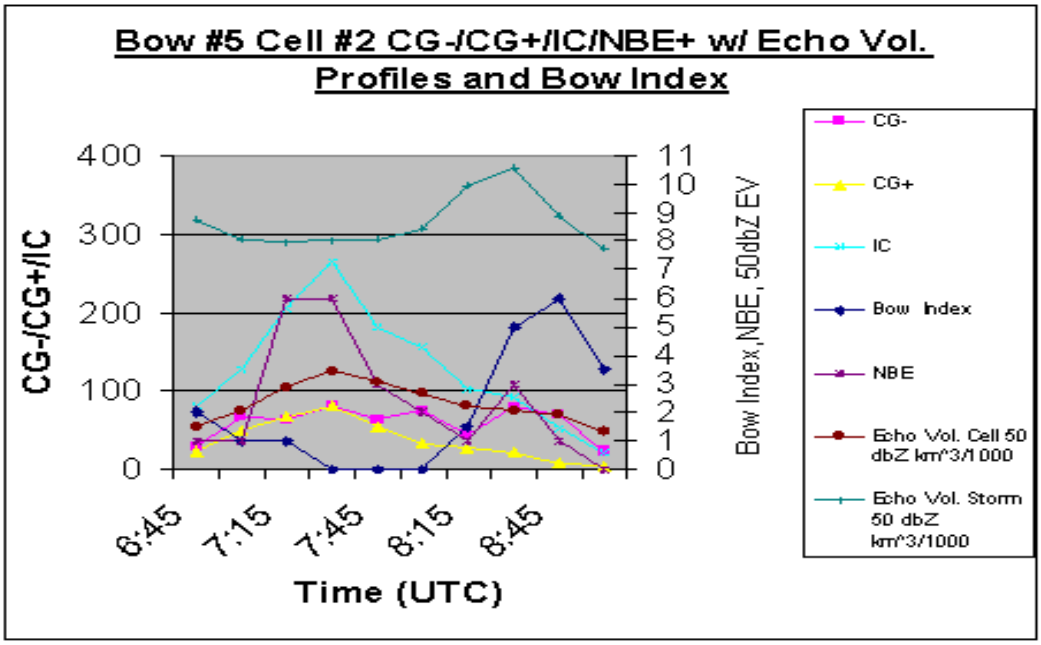

Figure 4.12: Lightning and Echo Volume Characteristics for Cell#2 found in Bow Echo Case #5. The left Y-axis is plotting CG-/CG+ and IC lightning. The Right Y-axis is plotting 50 dbZ Echo Volumes (units given), +NBE, and bow index on a unitless 1-10 scale.

4.2 Tornadic Supercell Results

We examine five supercell cases in this section, ranging in location from southwest Nebraska to central Texas. A consistent trend has appeared within this small data set, in regards to the lightning characteristics just prior to, during and immediately following the time of tornado occurrence, referred to as TOT. We can also consider trends in Echo Volume relative to the TOT. Overall, the EV data collected reflect the violent nature of these storms, with normalized 50 dBZ Reflectivity Volumes ranging between $2x10^3$ and $2x10^4$ km^3. These numbers agree well with previously reported values from STEPS 2000 where values ranged from 2-7 $x10^4$ km^3 for an entire supercell. (Tessendorf et al. 2007). Also, CG+ flash rates were reasonable, all supercells defined as possessing high-density positive lightning. (> .01 flashes/km^2/hr) (Stolzenburg 1998).

Lastly, NBE+ frequencies were not consistent from case to case. Possible explanations for this discrepancy will be discussed in more detail.

4.2.1 Supercell Case #1: F0 Tornado 2-3 June 2005.

At 22:30Z on 2 June, a very intense isolated supercell developed across the northeastern Colorado Plains, and an associated weak tornado was spotted at approximately 0:30Z, staying on the ground for approximately 15 minutes. Note that a 40 dBZ Echo Volume profile (EV) was used in Figure 4.13, due to an erratic 50 dbZ Reflectivity Volume parameter. Prior to the tornadic time period (TOT), the lightning characteristics in Figure 4.13 suggest that the storm strengthened from 22:30Z-23:15Z given a slowly rising IC lightning rate and NBE+ frequency, coupled with decreases in overall CG flash rate. Past research has exhibited that a strong correlation exists between storm intensity and IC/CG ratio (Boccippio 2002). The 40 dBZ EV Profile supports this hypothesis as does comparative radar PPI images from 22:30Z and 23:15Z, respectively (Fig. A.39). From 23:15Z-23:45Z, it is difficult to conclude trends. Falling NBE+ rates plus increases in CG- and CG+ relative to IC lightning might suggest a weakening, however the 40 dBZ EV shows essentially no change in intensity. The radar images at 23:15Z (Fig. A.39) vs. 23:45Z (Fig. A.40) appear similar. From 23:45Z -0:30Z there is consistent intensification, with peak 40 dBZ Echo Volume occurring at the onset of the TOT. Increasing CG+ support this claim, as noted in prior research campaigns (Tessendorf et al. 2007). NBE+ rates peak slightly earlier than 0:30Z, however rates remain rather high pre tornado at 3-4/min. During the TOT, all lightning parameters experience a sharp decrease. A slight weakening based on 40 dBZ EV is noted. Post tornado, from 0:45Z-2:00Z, the storm reinvigorates and continues to intensify based on a

steadily increasing 40 dBZ EV. Although the traditional lightning parameters increase in frequency over this time-span, the NBE+ rates post tornado do not reach flash rates seen prior to the tornado.

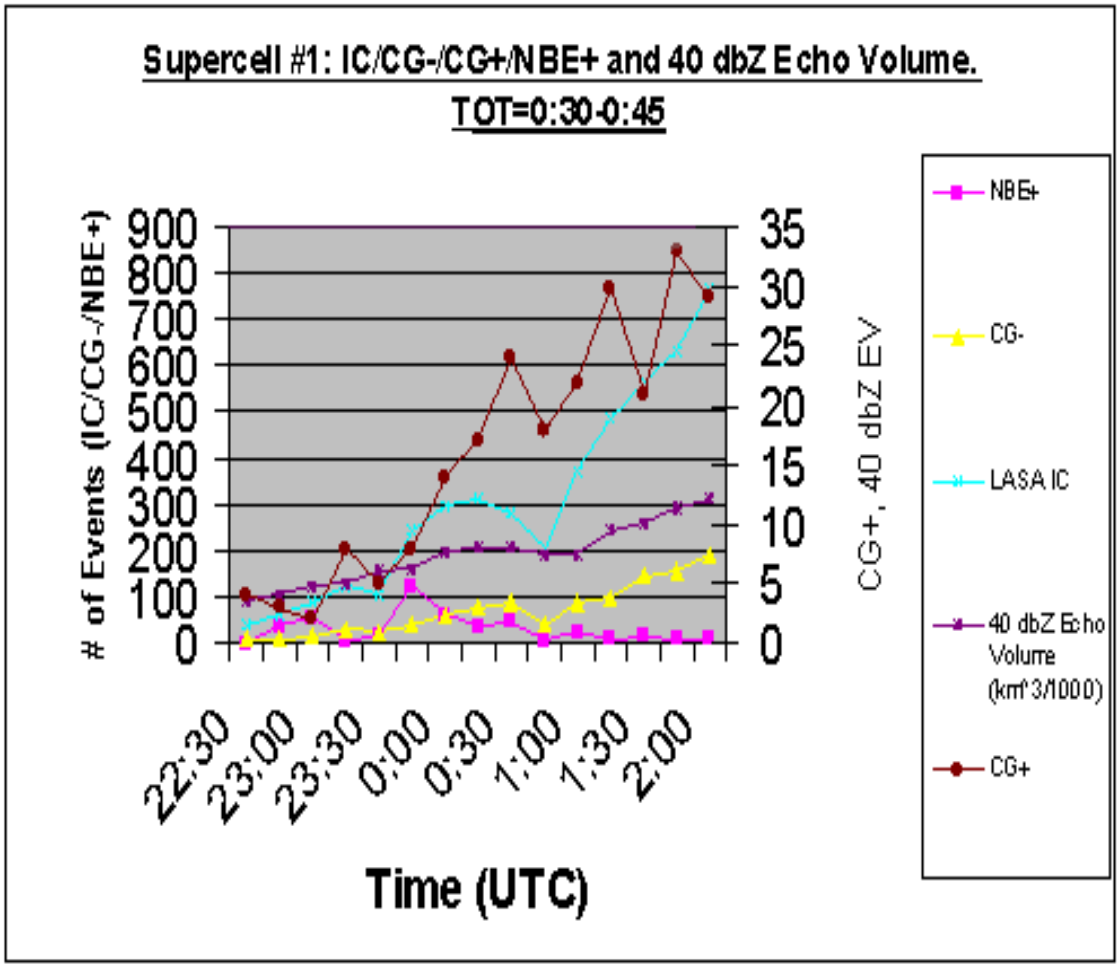

Figure 4.13: Lightning and 40 dbZ Echo Volume Characteristics of Supercell #1 on 2-3 June 2005. Time of Tornado denoted by TOT. The Left Y-axis is plotting IC/CG-/NBE+. The Right Y-axis is plotting CG+ and 40 dBZ EV.

4.2.2 Supercell Case #2: F1 Tornado on 11 May 2005.

At 20:45Z on 11 May 2005, two small supercells traveling nearly due north alongside one another, merged to form a larger, stronger supercell. Just an hour later, at 21:45Z-22:00Z a tornado was generated and confirmed by spotters. Leading the tornado, the 50 dBZ Echo Volume in Figure 4.14 suggests that the supercell intensified modestly over the first 30 minutes, then proceeded to rapidly strengthen until the onset of the time of tornado (TOT). The lightning data additionally reinforces this quantitative measure, as reflected by the sharply increasing IC/CG ratio noted just prior to the TOT (Boccippio 2002). Interestingly, NBE+'s started to occur only after the more distinct intensification began. During the Tornado time period, a marked decrease in convective strength was noted in the 50 dBZ Echo Volume with this downward trend continuing for 30 minutes post-tornado. Radar images pre and post tornado exhibit this event (Fig A.41 and Fig. A.42). All of the traditional lightning parameters (IC/CG-/CG+) dropped from 21:45Z-22:00Z, then quickly rebounded following the tornado. These lightning characteristics lend further credence to a weakening phase. Although these lightning parameters were increasing, from 22:00Z-22:30Z the IC/CG ratio is still lower than it was prior to the tornado. The marked increase in IC lightning, combined with an increasing 50 dBZ EV from 22:30Z-23:00Z, confirms an intensification. Increasing CG+ and NBE+ parameters offer additional support for intensification based on past research (Tessendorf et al. 2007, Wiens et al. 2008). Curiously, the NBE+ frequency experienced a maximum within the tornado time period itself, and not in conjunction with the rest of the lightning parameters. However, previous research has shown the +NBE to slightly lag peak convective strength in some cases (Wiens et al. 2008).

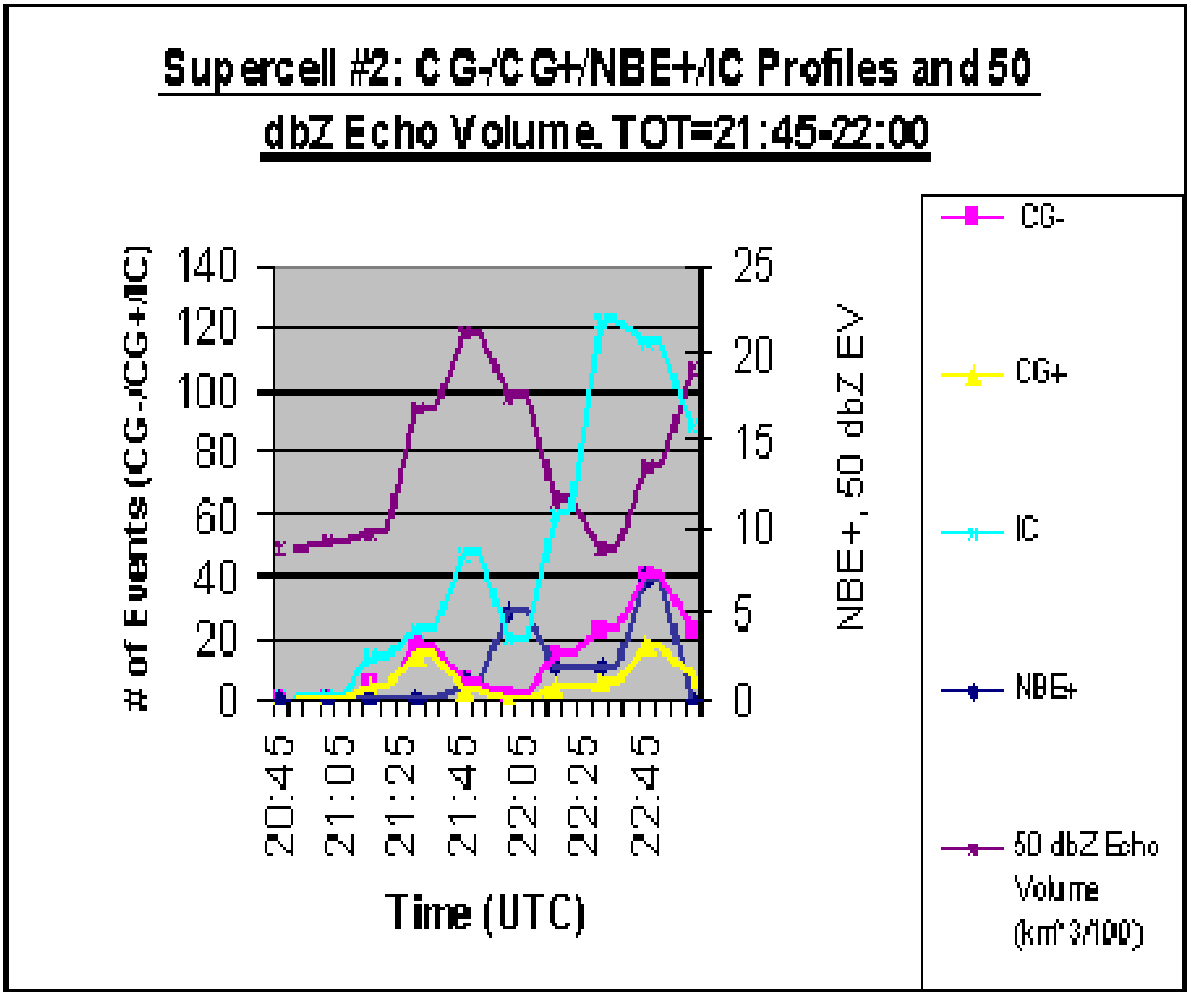

Figure 4.14: Lighting and Echo Volume Characteristics for Supercell #2 on 11 May 2005. TOT denotes the time of tornado. Left Y-axis is plotting CG-/CG+/IC. Right Y-axis is plotting +NBE, and 50 dBZ EV (units given).

4.2.3 Supercell Case #3: F1 Tornado on 13 May 2005.

At 21:00Z on 13 May 2005, a strong supercell previously associated with a squall-line bow echo, tracked south across the southeast corner of the Texas panhandle, rapidly intensifying before producing an F1 tornado from 22:20Z-22:30Z. As mapped by the 50 dBZ Echo Volume in Figure 4.15, the supercell strengthened quickly from 21:15Z-21:45Z, followed by a more subtle increase leading to the tornado time period, or TOT. Radar PPI images at 21:15Z and 21:45Z indicate a strong intensification (Fig A. 43

and Fig. A.44). The lightning characteristics also indicate a consistent intensification leading the tornado, as evidenced by a distinct increase in IC lightning relative to a more slowly increasing CG- flash rate; an increasing IC/CG ratio. CG+ flash rates in this cell are small. At the time of tornado, IC and CG- flash rates plummet. Interestingly, the 50 dBZ Echo Volume at TOT did not drop, as was noted in Supercells 1 and 2. While this feature could be a result of the 50 dBZ Echo increasing near the surface, but decreasing in the upper levels of the supercell, the EV profile is limited in its ability to account for the distribution of a given reflectivity. Following the tornado, the cell begins a more distinct strengthening period as seen in the 50 dBZ EV. While CG- rates increase immediately and lend support to this strengthening based on the findings of Suszcynsky and Heavner (2003), IC lightning appears to be delayed slightly in comparison to both CG parameters. This may be a direct result of the strengthening updraft trying to rebuild mid and upper level charge following the tornado. Amazingly, there are no NBE+'s in this cell, despite the fact that this cell, at least in terms of 50 dBZ EV, is stronger than either of the two previous cases.

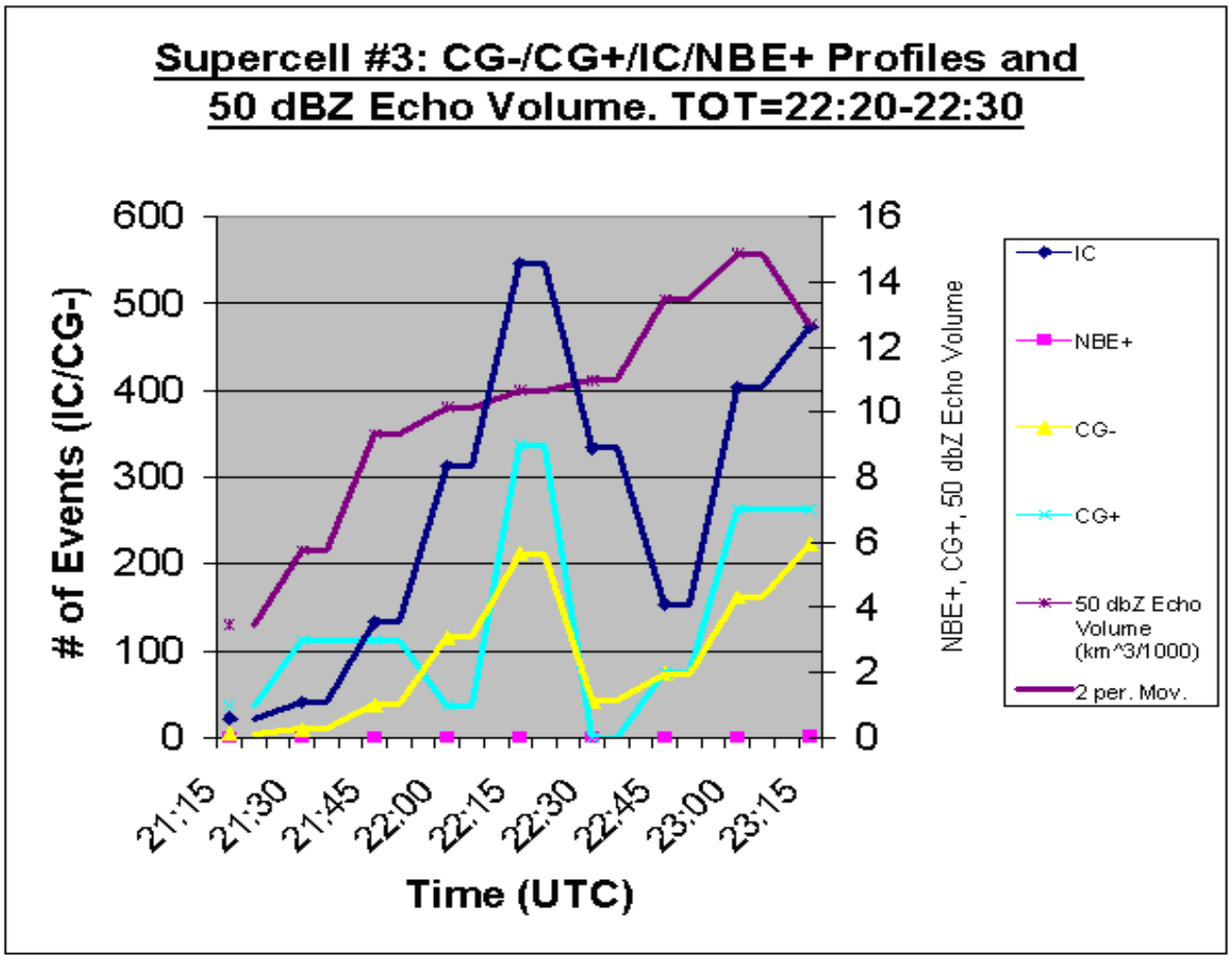

Figure 4.15: Lightning and Echo Volume Characterstics for Supercell Case #3 on 13 May 2005 from 21:15Z-23:30Z. TOT denotes the time of tornado. Left Y-axis is plotting IC/CG-. Right Y-axis is plotting CG+, NBE+ and 50 dBZ Echo Volume (units given).

4.2.4 Supercell Case #4: F3 Tornado on 2 June 2005.

At 21:30Z a rapidly moving area of convection exploded in intensity just southeast of the Denver Metro Area, and raced east-northeast, rapidly strengthening and producing a powerful F3 Tornado, which descended to the ground just before 22:45Z. As seen in Figure 4.16, from 21:30Z-22:45Z, the 50 dBZ Echo Volume strongly increased over this time frame, denoted a rapid intensification. The corresponding radar images confirm this feature (Fig.A.45 and Fig. A.46). Lightning data was difficult to interpret

over this time period, given a low IC lightning rate in comparison to the CG- flash rate. It is unrealistic to believe that a storm of this magnitude would have exhibited IC/CG ratios less than 1. The depressed IC returns for this specific case were likely a result of storm placement at the edge of the LASA network. Therefore, the IC lightning characteristics could not be used to support the findings of the radar and EV profile. At the time of tornado, CG- and CG+ both decreased in frequency and remain depressed in number until approximately 23:00Z following the tornado (Figure 4.16). The 50 dBZ Echo Volume was also slightly depressed over the TOT. Interestingly, no +NBE's were seen prior to or during the tornado. Only after TOT, did NBE+ events occur alongside traditional lightning parameters. Post-tornado, the storm slowly strengthened from 23:00Z-23:30Z as indicated by the 50 dBZ Echo Volume. In support of this claim, the IC flash rate began to quickly exceed that of the total CG flash rate. Particularly after 23:15Z, the IC/CG ratio become a much more realistic value for this storm type, with IC flash rates on the order of 10/min and an IC/CG approx. 6:1 (Boccippio 2002). It may have been the case, that as this cell progressed eastward, it moved into an area of improved LASA Network coverage. NBE+ events skyrocketed at this point, peaking at a rate unmatched by the other supercell cases; around 12/min.

4.2.5 Supercell Case #5 F1 Tornado on 9-10 June 2005.

At 23:00Z a strong area of convection developed in southwest Kansas and tracked northeast. A classic supercell with hook echo proceeded to form, producing a modest tornado from 0:00Z-0:15Z. Of note, this cell was by far the most electrically active case in this study. From 23:00Z-0:00Z, the 50 dBZ Echo Volume increased, rapidly over the

first 30 minutes, then slightly over the next half hour (Figure 4.17). A distinct rise in IC lightning flash rate coupled with slower increases in both CG lightning

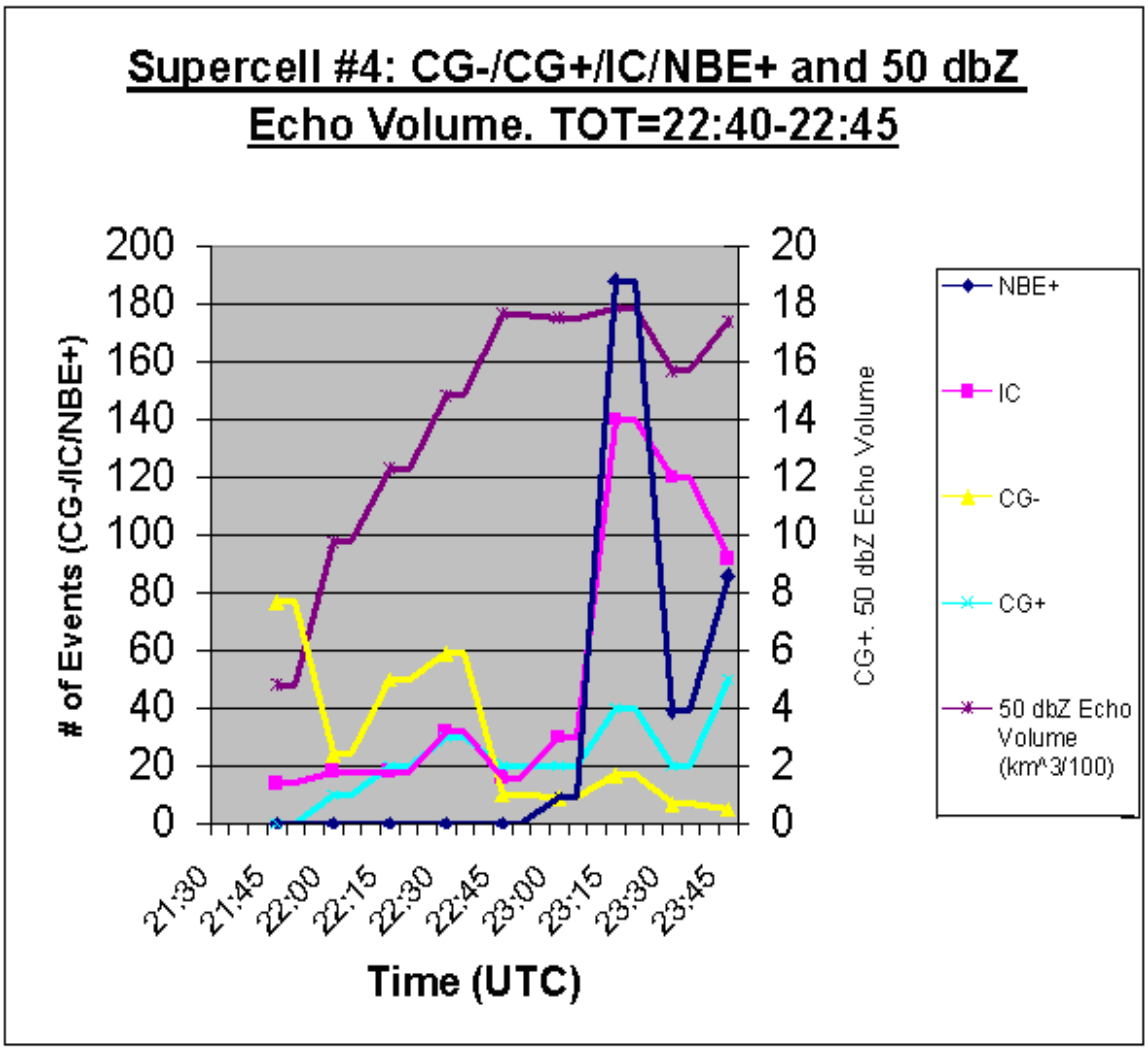

Figure 4.16: Lightning and Echo Volume Characteristics for Supercell Case #4 on 02 June 2005 from 21:45Z-0:00Z. The Left Y-axis is plotting CG-, IC, and NBE+. The Right Y-axis is plotting CG+ and the 50 dBZ EV (units given).

parameters produced an increasing IC/CG ratio, indicating the presence of a developing supercell (Boccippio 2002). IC flash rates prior to the tornado peaked at approx 5.3 fl/km^2/hr. CG+ flash rates maximized at about 70 per 5 min, in-line with previously

reported values for strong supercell storms (Stoltzenburg et al. 1998). The total percentage of CG+ vs total CG was approximately 45% at 0:00Z. Despite having the most impressive appearance on radar, this supercells' 50 dBZ Echo Volume was not the largest seen among all cases, and in fact was only 1/3rd of the 50 dBZ EV seen for Supercell #3. NBE+'s followed the characteristics of the traditional lightning parameters fairly well during this time. During the Time of Tornado (TOT), there was a marked drop in every lightning type. IC flash rates dropped to approx. 0.8 fl/km^2/hr. A corresponding decrease in 50 dBZ Echo Volume was also noted. In comparison to the other cell cases, this supercell experienced the longest delay between the end of the tornado and a subsequent re-intensification. From 0:15Z-0:45Z, a continued decrease was seen in the 50 dBZ Echo Volume. Furthermore, all lightning rates remain suppressed over this time, particularly in terms of IC lightning. NBE+ rates were less than 1/min. From 12:45Z-1:15Z, the cell finally began to reintensify, based on the 50 dBZ EV and supporting radar images As noted by past research, increases in +NBE's over this timeframe additionally serve to support this idea (Wiens et al. 2008). By 1:15Z nearly 75% of all CG lightning is positive, typical of a strong supercell (Stolzenburg et al. 1998). In this case, the presence of the tornado likely affected the storm dynamics and thus the ability for the supercell to quickly reintensify.

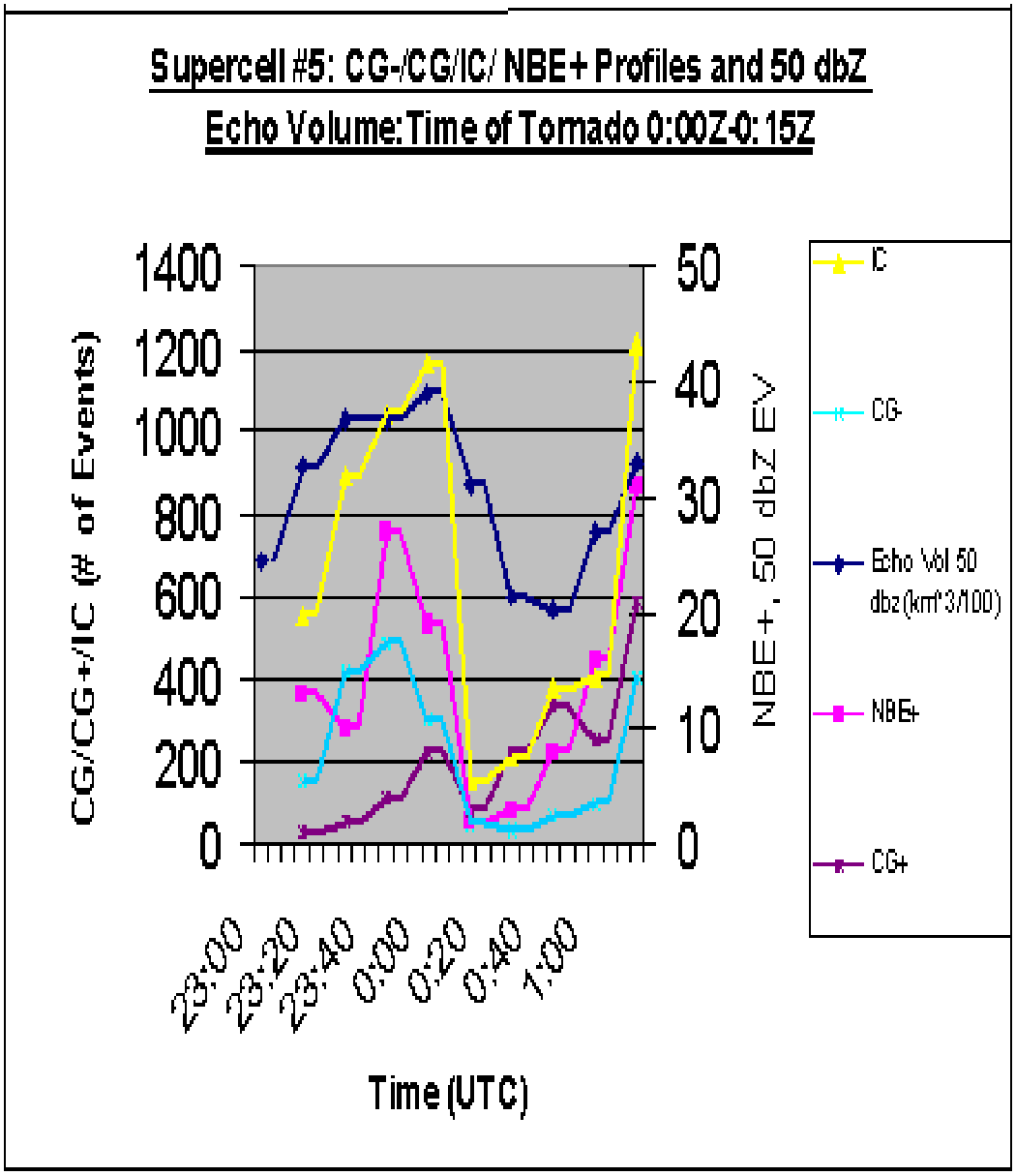

Figure 4.17: Lightning and Echo Volume Characteristics for Supercell Case #5 on 9-10 June 2005 from 23:15Z-1:15Z. The Left Y-axis is plotting CG-/CG+/IC. The Right Y-axis is plotting +NBE and 50 dBZ EV.

4.3 CAPE and Shear Profile Results

Of interest regarding the supercell results, was to answer why there was such a strong discontinuity in NBE+ frequency. Given storms of similar 50 dBZ Echo Volume and overall size, NBE+ event rates exhibited a broad spectrum. Initially, it was thought that there might be a latitudinal variance in NBE+, in connection with higher CG+ flash rates at the more northerly latitudes, specifically over the NE Colorado High Plains (Zajac and Rutledge 1990). At least for this storm set, that notion proved to be unfounded. The findings of Wiens et al. (2008) exhibited that not all storms produce +NBE's, regardless of storm strength, but showed that the strongest convection statistically has more +NBE occurrences. When the thermodynamic variables of Convective Available Potential Energy (CAPE) and 0-6 km Shear were collected for each supercell, no distinct relationship surfaced regarding more favorable storm environments producing higher +NBE rates. Therefore, no conclusive statements can be made regarding these results.

Chapter 5

DISCUSSION

5.1 Discussion of Bow Echo Results

5.1.1 Traditional Lightning Parameters in Both Bow Types

Based on the results obtained for both the uni-cell and squall-line bow types, a number of the primary research goals presented earlier may now be addressed. Specific to the bow echo as a whole, this research sought to determine if a connection existed between lightning activity and the bowing of the storm. Additionally, the question was posed whether or not lightning activity would be a function of bow type (squall type or uni-cell). In terms of total lightning activity and its relationship to the physical bowing of the storm, it appears that regardless of bow type, the actual bowing does not play a significant role in inducing increases in any of the traditional lightning parameters. It was thought that lowering of charge to the ground via a consistently strengthening rear-inflow jet might be the mechanism at work, but rather the strongest correlation exists between lightning activity and the convective strength of the overall storm. A previous study noted maximums in CG+ relative to bow peak in a cell embedded within a larger bow echo (Lang and Rutledge 2006). This finding was an impetus for examining whether this feature would pertain to a complete bow echo system. However, this behavior was not seen in the bow cases analyzed.

Instead, the data exhibited that the total lightning patterns seen, regardless of bow type, were consistently a reflection of the bow convective strength, with the bow being a result of the convective strengthening. Furthermore, based on the correlation of the 50 dBZ Echo Volume, Radar PPI images and various lightning convective strength proxies, this maximum of radar-inferred bow convective strength repeatedly preceded the bow index maximum. The time between the bow echoes' peak convective strength and the bow index maximum, ranged from 15 to in some cases 45 minutes. While this distribution is a curious result, the lag seen in these two fields can perhaps be explained via the findings of Weisman (1993), who performed bow echo simulations. In relating storm strength to radar-based storm appearance, the study showed that as the cold pool strengthened, the primary updraft was forced upright due to a vorticity balance, and a period of convective strengthening ensued. Further in this development the rear inflow began to intensify, a physical bowing of the convective line appeared, and the updraft remained vertical. By the final timepoint of the Weisman analysis, the rear inflow had increased to such a degree that it extended all the way to the front of the convective line. At this point, the simulation visually represents a well-developed bow echo. Although, the storm updraft was stronger in magnitude at this final time, it appeared to be tilted slightly upshear at this juncture (Weisman 1993). A rear-inflow descent to the surface at this time additionally further impinged on the primary updraft. Therefore, the storm convective strength experienced a maximum just prior to the point at which the rear-flow descended, promoting a bow maximum, but simultaneously tilting the primary updraft due to an imbalance in vorticity, thus weakening the bow to a slight degree. The degree of lag seen may be a function of storm size, as the uni-cell bow convective strength

maximums experienced a smaller delay relative to the larger squall-line bow cases. Although a viable explanation has been presented, it is still the case that the bow indices were assigned subjectively. Therefore, a degree of error may be present in this index.

5.1.2 Individual Cell Lightning Characteristics

Within the broader view of the squall-line bow echo, an important research question was to characterize the lightning behavior and trends associated with the individual cellular components of the overall squall-line. Furthermore, the relative contribution of these cells to the overall lightning activity and convective strength were to be characterized. Overall, the cells analyzed behaved similarly to the overall convective line a majority of the time, in that when the overall storm strengthened via the 50 dBZ Echo Volume, so did the cell. As these cells were located within the overall convective line, it was not unexpected that their individual behavior would be reflective of the entire line. In general, higher IC/CG ratios and increased CG+ flash rates were well correlated to the matching increases in reflectivity volume. The cell on an individual basis contributed to, but was never a key component of the overall flash rate for any of the traditional lightning parameters, given the relative percentage of lightning being generated from each cell compared to the entire storm. Surprisingly, even in cases where these cells acted in combination, they did not constitute a majority of the overall lightning (ex: Bow Echo Case #2). However, it should be noted that not all cells in the convective line were analyzed. Therefore, the overall contribution and effect from all cellular lightning cannot be broadly concluded from this study alone. What is most striking from these results, is the fact that a majority of these individual cells actually maximized in strength and lightning activity prior to the time point at which the overall bow

experienced its peak convective strength. Once again, there appears to be a lag, this time between cellular and overall bow convective strength. Also of interest, the smallest squall-line case, in terms of linear length, experienced the smallest delay between these two fields, while the largest in size had a greater time gap, upwards of 30-40 minutes. Regardless of the time gap, these premature spikes in lightning, did not appear to constitute a large enough flash rate to adversely change the overall storm lightning profile.

To support the cellular features noted, Weisman (1993) provides a possible explanation. It was noted in his study, that at the 120 min model time-point the bow was intensifying, yet the deepest parcel ascent was occurring in "more isolated cells outside of the zone defined by the bookend vortices". In this way, these individual cells were very intense at this time-point. While the Weisman case is more of an individual cell bow type, the fact remains that at the next time-point reported, the point at which the overall storm reached its maximum strength, nothing is reported in terms of further strengthening in these outlying cells. As these individual cells do not constitute a large portion of the overall storm in terms of reflectivity area, it is feasible to say that although these cells may not continue to strengthen over the final 15 to 45 minutes prior to the overall storm convective strength maximum, the overall line reflectivity apart from these cells can still increase and mask the lesser effects of these individual cells. A dynamic connection relating cell convective strength and overall storm strength may not be determined via the findings of this research alone. As most of the cells reported followed this trend, a few of the cases were unique in that they additionally experienced increases in convective strength/lightning activity when the storm was decidedly in a weakening phase. While

most of the spurious lightning features connected to these cells remained undetected by the overall storm lightning profiles, this feature was plainly evident in Bow Echo Case #4, where all of the cell cases analyzed experienced Echo Volume increases across an identical timeframe when the overall storm was weakening. This was the only timepoint across all cases, where the overall lightning profile was significantly influenced by a group of cells acting together in opposition of the overall storm.. Thus, individual cells largely act in conjuction with, but also at times can act independently from the greater storm either alone, or in coordination with one another.

5.1.3 NBE Characteristics in Bow Echoes

A related research goal for the bow echo was to characterize the behavior of the +NBE in these storms and determine if any trend or correlation could be developed between the +NBE and storm convective strength. Specific to the individual cell bow cases, it is difficult to see a distinct trend in terms of +NBE behavior. Bow Case #3 simply had little to no NBE activity. In terms of Bow Case #1, the NBE+ parameter generally increased as the storm increased in convective strength (maximum of 30 per 15 minutes), remained fairly constant during the storm's strongest phase, and then decreased as the overall storm weakened. However, it is evident that the NBE+ trend was more jagged and randomized in comparison to the traditional lightning parameters. The majority of both IC lightning and +NBE's were found in the same locations; namely within the bookend vortices. Given that the bookend vortices appeared via reflectivity estimates to be the strongest convective portions of the storm, this result was expected. So why did the +NBE not follow the lead of its IC counterpart given similar locations and reacting to similar dynamical changes?

The choice that was made in this analysis to monitor the +NBE at 15 min time intervals may have been a primary cause for this problem, in several instances being the direct cause for anomalous spikes in NBE+ frequency. For example, when a reanalysis of the 6:30Z-6:45Z time was conducted in Bow Echo Case #1, it was found that all of the NBE+ recorded during the time-period occurred in the first five minutes. The following ten minutes had no +NBE's and large drops in lightning flash rate. Overall, the timeframe based on 50 dBZ Echo Volume and corresponding radar images registered as a period of weakening (Fig. A.47 and Fig. A.48). The NBE+ rate spiked because of this short burst of intensification but did not match the other parameters over the entire timeframe.

Secondly, the data shows both in the individual cell and squall-line cases, significant jumps in +NBE rate accompanying the strongest rate increases in convective strength. While in most of the cases, the endpoint of rapid intensification and maximum convective strength were identical, in Bow Echo Case #1, there are several instances where the +NBE spiked during a period of rapid strengthening prior to the convective strength maximum, then decreased afterward even though the storm strengthen, though at a more modest rate. This hypothesis does not mean to explain all the fluctuations seen, but the number of times this effect was noted serves to perhaps support further investigation of this trend. Overall, this caused the +NBE trend to appear less definitive. Lastly, the research of Wiens et al. (2008) served to show that the +NBE is simply not consistent in terms of its appearance in strong convection. The wavering +NBE trend seen could be explained via these findings alone applied to the uni-cell bow echo.

In relation to the squall-line bow type, it is apparent that the +NBE primarily occurs within the individual cells located within the broader convective line (Fig. A.49).

There appears to be no trend in terms of cell location within the line and NBE+ rate. Due to the fact that the +NBE is primarily driven by the decreases/increases in cell strength, the pattern of the +NBE when viewed as part of the overall bow, did not appear as a smooth trace but fluctuated as the individual cells strengthened and weakened. While most obey the trends previously discussed, a random rogue individual cell, or a group of cells acting in coordination were shown in several instances to markedly change the overall NBE+ profile. This effect can be noted in Figure 4.4 at 7:30Z. Also, one should note that although the 50 dBZ EV's were similar for each squall-line bow, bow #4 produced basically no +NBE's in comparison to the other two cases. Overall, the NBE+ does not appear to be a reasonable proxy for use as a predictor of storm bowing, however traditional lightning parameters appear to be well suited for this application, as discussed previously.

5.2 Discussion of Tornadic Supercells

5.2.1 Total Lightning Characteristics

In general, each of the tornado supercells analyzed, regardless of tornado strength, exhibited very similar lightning characteristics. As expected, the total lightning mimicked the convective strength of the supercell (Goodman et al. 1988).

Prior to the time of tornado, each case was associated with an intensification period, as denoted by the 40/50 dBZ Echo Volumes. Just prior to the tornado confirmation, each storm underwent a small period of weakening or steady state accompanied by marked drops in lightning rates. This depression was consistent, and was immediately followed by subsequent varying degrees of re-intensification. Lightning rates generally rebounded in this post-tornado storm strengthening phase. Unfortunately,

the total lightning "dip" seen does not match either of the expected profiles put forth by Macgorman and Rust; hereafter denoted by MR (1998). While Macgorman and Rust showed cases where CG flashes were slightly delayed from the Time of Tornado (TOT), the IC flash rate conversely increased at the TOT. For weak tornado cases shown in MR, both lightning types increased at the TOT. To address this issue, it should be first be noted, that while MR have given these examples, there are wide variations in supercellular lightning characteristics reported within the literature. In support of the herein results, one can apply the findings of Goodman et al. (1988) towards the characteristics noted. The literature has shown that tornadoes are most likely to occur during the phase of supercell collapse (Brandes 1978). Goodman et al.'s study of general supercell dynamics exhibited that during supercell collapse, lightning rates decreased dramatically. This feature is reflected by all of the case examined here. Additionally, during this stage, there is a large amount of mass and momentum descending to the ground. Perhaps, this descent was able to slow the primary updraft for a period of time, such that the storm weakened. The fact that the 50 dBZ Echo Volume either decreased or flattened during the TOT in every case would lend support to this dynamic explanation.

5.2.2 Supercell +NBE Characteristics

Overall, the +NBE characteristics of these tornadic supercells were highly inconsistent and provide very little support for using the +NBE as a convective strength proxy for these case types. Some cases had essentially no +NBE's present, although 50 dBZ Echo Volume and overall size were similar in quantity to those cases that had much higher +NBE rates. Other cases experienced no +NBE activity prior to the tornado despite being very intense cells, then responded with appreciable +NBE counts only

during and after TOT. Some were exactly reversed, with +NBE's prior to but severely decreasing after the TOT, despite storm intensification post-tornado. When +NBE's did occur they followed the convective strength pattern of the storm, but this did not happen with any degree of consistency. Unlike the bow echo cases, +NBE rate does not appear to be a function of the rate change of convective strength, but instead is characteristically more random. The findings of Wiens et al. (2008) would serve to support the inconsistent nature of the +NBE within each individual storm.

5.3 Conclusion

The total lightning characteristics of the bow echo cases analyzed, regardless of type, exhibit consistency in that their lightning statistics correlate well against the convective strength of the storm. Repeatedly the convective strength and lightning maximums precede the bow maximums by an appreciable period of time, on the order of 15 to 30 minutes. Therefore, the bow itself does not appear to directly play a mechanistic role in physically enhancing the total lightning flash rate. The prospects of using these findings (flash rate, flash type), as a forecasting tool for bow echo maximums and associated wind damage should be further investigated. The individual cellular components within the squall-line bow echo exhibit lightning characteristics similar to the broader storm and furthermore exhibit intensity maxima preceding the overall storm strength maxima. While an individual cell does not appear to be capable of directly influencing the overall storm lightning activity or related EV, a number of cells acting in coordination, and in opposition to the overall storm trend do possess the ability to change the overall storm lightning profile. These cells show a degree of random variability in their behavior, although a majority of the time they act in concert with the overall storm.

As these convective components are the primary source of +NBE's in this storm type, the functionality of using the +NBE as a proxy for squall-line bow strength has not been justified. Rather, the +NBE could be better applied to more accurately monitor an individual cell within, given an appreciable +NBE event rate.

The uni-cell bow cases, given favorable storm environmental parameters and higher data acquisition rate on the order of 5 minutes or less, might be better suited towards using the +NBE as a storm strength and perhaps more importantly, a proxy for intensification rate. As the LASA data offers +NBE data at 5 minute intervals, an investigation towards the improvement of +NBE trends could easily be accomplished. Unfortunately, the inherent nature of the +NBE as an unreliable proxy has not been refuted for this specific case type.

The supercell total lightning cases exhibit a repeatable depression in lightning rate just prior to and during the time of tornado. A possible explanation of this phenomenon has been offered, but bears further scrutiny. The +NBE characteristics of these storms are quite erratic, lending to the inability of the +NBE as a valid storm proxy. Obtained results were not able to validate a connection between +NBE frequency and the gross environmental scene.

Tornado strength has not been connected to +NBE frequency in this data set. Certainly, an analysis of more storms over a larger geographic area, would be necessary to further support and verify some of the initial findings made in this report.

REFERENCES

Barnes, S.L., 1978: Oklahoma Thunderstorms on 29-30 April 1970. Part I: Morphology of a tornadic storm. *Mon. Weather Rev.*, **106**, 673-684.

Bernardet, L.R. and W.R. Cotton, 1998: Multi-Scale Evolution of a Derecho Producing Mesoscale Convective System. *Mon. Weather Rev.,* **26**, 2991-3015.

Biagi, C.J., K.L. Cummins, K.E. Kehoe, E.P. Krider, 2007: NLDN Performance in Southern Arizona, Texas and Oklahoma in 2003-2004. *J. Geophys. Research*, **112**, D05208.doi:10.1029/2006JD007341

Bluestein, H.B., D.R. Macgorman, 1998: Evolution of Cloud-to-Ground Lightning characterstics and storm structure in the Spearman, TX Tornadic Supercells of 31 May 1990. *Mon. Weather Rev.,***126**, 1451-1466.

Boccippio, D.J., 2002: Lightning scaling relations revisited. *J. Atmos. Sci*.,**59**, 1086-1104.

Brandes, E.A., 1978: Mesocyclone Evolution and tornadogenesis: Some observations. *Mon. Weather. Rev.*, **106**, 995-1011.

Brooks, E.M., 1949: The tornado cyclone, *Weatherwise*, **2**, 32-33.

Browning, K.A., 1964: Airflow and precipitation trajectories within severe local storms which travel to the right of the wind. *J. Atmos. Sci.,* **21**, 634-639.

Burgess, D.W., R.A. Brown, L.R. Lemon, C.R. Safford, 1977: Evolution of a tornadic thunderstorm. *Preprints: Tenth Conf. On Severe Local Storms*, Omaha, Amer. Meteor. Soc.,84-89.

Burke, P. and D. Schultz, 2004: A four-year climatology of cold season bow echoes over the continental United States. *Weather and Forecasting*, **19**, 1061-1074.

Byers, H.R., 1942: Non-Frontal Thunderstorms. *Misc. Rep. No.3*, Chicago: Univ. Chicago Press, 26 pp.

Carey, L.D., S.A. Rutledge, W.A. Petersen, 2003: The relationship between severe storm reports and Cloud-to-Ground Lightning Polarity in the contiguous U.S. from 1989 to 1998.

Cummins, K.L., M.J. Murphy, E.A. Bardo, W.L. Hiscox, R.B. Pyle, A.E. Pifer, 1998: A combined TOA/MDF Technology Upgrade of the U.S. National Lightning Detection Network, *J. Geophys. Res.,* **103(D8),** 9035-9044.

Davies-Jones, R., 1984: Streamwise Vorticity: The Origin of Updraft Rotation in Supercell Storms. *J. Atmos. Sci.*, **41**, 2991-3006.

Fujita, T.T., 1978: Manual of Downburst Identification for project NIMROD. Technical Report, Dept. of Geophysical Sciences, Univ. of Chicago, Chicago, IL.

___ 1959: Precipitation and Cold-Air production in Mesoscale Thunderstorm Systems, *Journal of Meteorology*, **16**, 454-467.

____ and H. Grandoso, 1968: Split of a thunderstorm into anticyclonic and cyclonic storms and their motion as determined by numerical model experiments, *J. Atmos. Sci*., **25**, 416-439.

Goodman, S.J., D.E. Buechler, D.J. Meyer, 1988: Convective Tendency Images derived from a combination of lightning and satellite data, *Weather and Forecasting*, **3**, 173-188.

Grenet, G., 1947: Essay on the Explanation of Electrical Charge in Storm Clouds, *Ann. Geophysics*, **3**, 306-307.

Heymsfield, A.J., P.N. Johnson, J.E. Dye, 1978: Observations of moist adiabatic ascent in NE Colorado cumulus congestus clouds, *J. Atmos. Sci.*, **35,** 1689-1703.

Hilgendorf, E. and R. Johnson, 1998: A study of the evolution of meso-scale convective systems using WSR-88D data, *Weather and Forecasting*, **13**, 437-452.

Hitschfeld, W., 1960: The motion and erosion of convective storms in severe vertical wind shear, *J. Meteorology*, **17**, 270-282.

Huff, F.A., H.W. Hiser, S.G. Bigler, 1954: Study of an Illinois tornado using RADAR, synoptic weather and field survey data, *Rep. of Investigation No. 22*, Illinois State Water Survey, 73 pp.

Jacobsen, A.R., 2003: Relationship of intra-cloud lightning radio frequency power to lightning storm-height, as observed by the FORTE satellite, *J. Geophys. Res.*, **119**, 345-361.

____ and M.J. Heavner, 2005: Comparison of Narrow Bipolar Events with ordinary lightning as proxies for severe convection, *Mon. Weather. Rev.*, **133**, 1144-1154.

Kamburova, P.L. and F.H. Ludlum, 1966: Rainfall evaporation in thunderstorms downdrafts. *Quart. J. of the Royal Meteor. Soc*., **92**, 510-518.

Klemp, J.B. and R.B. Wilhelmson, 1978: Simuations of right and left moving storms produced through storm splitting, *J. Atmos. Sci.,* **35**, 1097-1110.

Klimowski, B., M. Hjelmfelt, M.J. Bunkers, 2004: RADAR Observations of the early evolution of bow echoes, *Weather and Forecasting*, **19**, 727-734.

_____, R. Przybylinksi, G. Schmocker, 2000: Observations of the formation and early evolution of Bow Echoes, *Preprints, 20th Conf. On Severe Local Storms*, Amer. Meteor. Soc., Orlando, FL, 44-47.

_____, M.J. Bunkers, J.N. Covert, 2003: Severe Convective Windstorms over the Northern High Plains of the United States, *Weather and Forecasting*, **18**, 502-518.

Krehbiel, P.R., J.A. Riousset, V.P. Pasko, R.J. Thomas, W. Rison, M.A. Stanley, H.E. Edens, 2008: Upward Electrical Discharges from Thunderstorms, *Nature Geosci.,* **1**, 233-237.

Kuetnner, J.P., Z. Levin, J.D. Sartor, 1981: Thunderstorm Electrification-Inductive or Non-Inductive, *J. Atmos. Sci*, **38**, 2470-2484.

Lang, T.J. and S.A. Rutledge, 2002: Relationships between convective storms, kinematics, precipitation and lightning, *Mon. Weather. Rev*., **130**, 2492-2506.

_____, 2006: Kinematic, Microphysical and Electrical Aspects of an Assymetric Bow Echo Mesoscale Convective System observed during STEPS 2000, EOS Trans. AGU, 87(52), Fall 2006 Meeting, Abstract AE33A-1057.

Lemon, L.R., 1970: Formation and emergence of an anticyclonic eddy with a severe thunderstorm as revealed by radar and surface data, *Preprints 14th Conf. On Radar Meteorology*, Amer. Meteor. Soc., Tucson, 323-328.

_____, 1976: The flanking line, a severe thunderstorm intensification source. *J. Atmos. Sci*., **33**, 686-694.

_____, and C.A. Doswell III, 1979: Severe Thunderstorm Evolution and Mesocyclone Structure as related to tornadogenesis, *Mon. Weather. Rev.,* **107**, 1184-1197.

Levine, D.M., 1980: Sources of the strongest rf Radiation from Lightning, *J. Geophys. Res*., **85**, 4091-4095.

Macgorman, D.A. and D.W. Rust, 1998: The Electrical Nature of Storms. Oxford University Press, pp. 250-253.

_____ and K.E. Nielsen, 1991: Cloud to Ground Lightning in a Tornadic Storm on 8 May 1986, *Mon. Weather Rev.*, **119**, 1557-1574.

_____, D.W. Burgess, V. Mazur, D.W. Rust, 1989: Lightning rates relative to tornadic storm evolution on 22 May 1981, *J. Atmos. Sci.*, **46**, 221-250.

Markowski, P.M., J.M. Straka, E.N. Rasmussen, 2002: Direct Surface Thermodynamic Observations within the Rear Flank Downdrafts of Non-Tornadic and Tornadic Supercells. *Mon. Weather Rev.*, **130**, 1692-1721.

Marwitz, J.D., 1972: The structure and motion of severe hailstorms, *J. Appl. Meteorology*, **11**, 166-179.

Newton, C.W. and J.C. Fankhauser, 1964: On the movements of convective storms, with emphasis on size discrimination in relation to water budget requirements, *J. Appl. Met*., **3**, 651-668.

Przybylinski, R. 1995: The bow echo observations, numerical simulations and severe weather detection methods, *Weather and Forecasting*, **19**, 203-218.

_____ and W. Gery, 1983: The reliability of the bow echo as an important severe weather signature. *Preprints, 13th Conf. on Severe Local Storms*, Amer. Meteor. Soc., Tulsa, OK, 270-273.

Rasmussen, E.N. and D.O. Blanchard, 1998: A Baseline Climatology of Sounding-Derived Supercell and Tornado Forecast Parameters, *Weather and Forecasting*, **13**, 1148-1165.

Ray, P.S., R.J. Doviak, G.B. Walker, D. Sirmans, J. Carter, B. Bumgarner, 1975: Dual-Doppler Observation of a Tornadic storm, *J. Appl. Meteor.*, **14**, 1521-1530.

Reynolds, S.E., M.Brook, M.F. Gormley, 1957: Thunderstorm charge separation, *J. of Meteorology*, **14**, 426-436.

Rison, W.R., R.J. Thomas, P.R. Krehbiel, T.Hamlin, J.Harlin, 1999: A GPS-Based three dimensional lightning mapping system: Initial observations in Central New Mexico, *Geophys. Res. Lett.*, **26**, 3573-3576.

Rutledge, S.A., C. Lu, D.R. Macgorman, 1990: Positive Cloud-to-Ground Lightning in Mesoscale Convective Systems, *J. Atmos. Sci.*, **47**, 2085-2100.

_____, E.R. Williams, T.D. Keenan, 1992: The Down Under Doppler and Electricity Experiment (DUNDEE): Overview and Preliminary Results, *Bull. Amer. Meteor. Soc.*, **73**, 3-16.

Rotunno, R. and J.B. Klemp, 1982: The influences of the shear induced pressure gradient on thunderstorm motion, *Mon. Weather Rev.*, **110**, 136-151.

_____, J.B. Klemp, M. Weisman, 1988: A theory for strong, long-lived squall lines, *J. Atmos. Sci.*,**45**, 463-485.

Schlesinger, R.E., 1975: A three dimensional numerical model of an isolated deep convective cloud, *J. Atmos. Sci.*, **32**, 934-957.

Shao, X.M., M. Stanley, A. Regan, J.Harlin, M.Pongratz, M. Stock, 2006: Total Lightning Observations with the new and improved Los Alamos Sferic Array (LASA), *J. of Atmos. and Oceanic Tech.*, **23**, 1273-1288.

Smith, D.A., X.M. Shao, D.N. Holden, C.T. Rhodes, M. Brook, P.R. Krehbiel, M. Stanley, W.R. Rison, R.J. Thomas, 1999: A distinct class of isolated intra-cloud lightning discharges and their associated radio emissions, *J. Geophys. Res.*, **104(D4),** 4189-4212.

Smull,B. and R. Houze, Jr., 1985: A mid-latitude squall line with a trailing region of stratiform rain: Radar and Satellite observations: *Mon. Weather Rev.*, **113**, 113-117.

Stoltzenburg, M., W.D. Rust, T.C. Marshall, 1998: Electrical Structure in Thunderstorm Convective Regions, *J. Geophys. Res*., **103**, 14097-14108.

Suszcynsky, D.M. and M.J. Heavner, 2003: Narrow Bipolar Events as indicators of thunderstorm convective strength, *Geophys. Res. Lett.*, **30**, 1879.
Takahashi, T., 1978: Riming Electrification as a charge generation mechanism in thunderstorms, *J. Atmos. Sci.*, **35**, 1536-1548.

Tessendorf, S.A., K.C. Wiens, S.A. Rutledge, 2007: Radar and Lightning Observations of the 3 June 2000 Electrically Inverted Storm for STEPS, *Mon. Weather Rev.*, **135**, 1-17.

Thompson, R.L., R. Edwards, J.A. Hart, K.L. Elmore, P. Markowski, 2000: Close Proximity Soundings within Supercell Environments obtained from the Rapid Update Cycle, *Weather and Forecasting*, **18**, 1243-1261.

Vonnegut, B., 1953: Possible mechanism for the formation of thunderstorm electricity, Bull. Amer. Meteor. Soc., 43, 378.

_____, 1955: Possible mechanism for the formation of thunderstorm electricity, *Geophys. Research Paper No. 42*, Proc. Conf. Atmos. Electricity AFCRC-TR-55-222, 169-181.

_____, 1963: Some facts and speculations concerning the origin and role of Thunderstorm Electricity, *Meteor. Monograms*, 5, 227.

Weisman, M. 1993: The genesis of Severe Long-Lived Bow Echoes, *J. Atmos. Sci.*, **50**, 645-670.

_____1992: The role of convectively generated rear-inflow jets in the evolution of long-lived mesoscale systems. *J. Atmos. Sci.,* **49**, 1826-1847.

_____ and J.B. Klemp, 1982: The dependence of numerically simulated convective storms on wind shear and buoyancy, *Mon. Weather Rev.,* **110**, 504-520.

_____, 1984: The structure and classification of numerically simulated convective storms in directionally varying wind shear, *Mon. Weather Rev*., **112,** 2479-2498.

_____, 1986: Characteristics of isolated convective storms, *Mesoscale Meteor. And Forecasting, Peter S. Ray Ed*., American Meteor. Soc., 331-358.

_____ and C. Davis, 1998: Mechanisms for the generation of mesoscale vortices within quasi-linear convective systems, *J. Atmos. Sci.,* **55**, 2603-2622.

Wiens, K.C., S.A. Rutledge, S.A. Tessendorf, 2005: The 29 June 2000 Supercell observed during STEPS. Part II: Lightning and Charge Structure, *J. Atmos. Sci*., **62**, 4151-4177.

_____, T. Hamlin, J. Harlin,D.M. Suszcynsky, 2008: Relationships among Narrow Bipolar Events, "total lightning", and radar-inferred convective strength in Great Plains thunderstorms, *J. Geophys. Research,* **113**, doi:10.1029/2007JD00940.

Wiens, K.C., *Personal communication*, 2008.

Willett, J.C., J.C. Bailey, E.P. Krider, 1989: A class of unusual lightning electric field waveforms with very strong high frequency radiation. *J. Geophys. Res.,* **94**, 16255-16267.

Williams, E.R., 1989: The tripole structure of thunderstorms, *J. Geophys. Res.,* **94,** 13151-13167.

_____, 2001: The Electrification of Severe Storms, *Severe Convective Storms, Meteor. Monograms,* No.50, Amer. Meteor. Soc., 527-561.

_____, S.G. Geotis, N. Renno, S.A. Rutledge, E. Rasmussen, T. Rickenbach, 1992: A Radar and Electric study of Tropical "hot towers", *J. Atmos. Sci.,* **49**, 1386-1395.

Zajac, B.A. and S.A. Rutledge, 2001: Cloud-to Ground Lightning activity in the contiguous United States from 1995-1999, *Mon. Weather Rev.,* **129**, 999-1019.